Response to Reviewer #1:

This paper presents another approach to handle the problem of lacking three dimensional training images for multiple-point geostatistical simulations. The authors explain the differences between their approach and previously existing ones and perform thorough sensitivity analyses on the new parameters required by their implementation. However, they take some prior important decisions that go unchallenged, such as the choice of the probability aggregation methods, and the parameters used in them. A sensitivity analysis of these decisions would provide a more solid basis for the usage of the new approach.

We are grateful for your insightful and constructive comments and suggestions. In order to more clearly present the probability aggregation strategy proposed in our paper, we moved the description of two existing formulas used in our work to a new section Background Information in the revised version (see P5L18-26 and P6L1-11). Thus the section 3.2 mainly focuses on the strategy for aggregating the pdfs from local sub-sections proposed in this work (see P9L7-22 and P10L1-13). The choice of the probability aggregation methods is described in P9L13-20. The sensitivity analysis of the weights of the probability aggregation formulas has been done in section 4.1.3 (see P18L2-16).

My major criticism is on the tests performed during the benchmarking. They are purely statistical, yet this is a journal very much related to surface and subsurface hydrology. Readers of HESS and potential users of this method would be more appealed to use it if the benchmark would include, for instance, some solute transport simulations.

Although this manuscript mainly focuses on the algorithm principle of reconstructing 3-D models of subsurface structures by using multiple-point geostatistical techniques, several data sets in hydrology or hydrogeology are used to test our methods, such as pore structure of sandstone (see section 4.1), folds in subsurface aquifers (see section 4.2), and a synthetic example: 3-D reconstruction of hydrofacies (see section 5). Therefore, we think that our method can be used to reconstruct 3-D models of complex heterogeneous structures in hydrology or hydrogeology and it meets the scope of HESS.

Response to Reviewer #2:

I read with interest the paper entitled "Locality-based 3D multiple-point statistics reconstruction using 2D geological cross-sections". The paper describes a new methodology to build 3D realizations constrained by 2D sections that act as local training images and hard data for MPS algorithms. The method seems to give realistic results and perform better than existing algorithms. Globally, the paper and the presented results are convincing. However, I would like the following general comments to be addressed by the author:

Thank you very much for your positive and constructive comments and suggestions. We have corrected all the issues you raised in the revised version. The following is a point-by-point response according to your comments.

1. The introduction is a little bit messy, giving an overview of many papers related to MPS, but missing the point of highlighting the specific issues tackled by the paper. For example, the 2nd paragraph (P2L15) makes the history of MPS. This is not the point, you should rather insist on the importance of the TI (what you do in paragraph 3) and the description of the state of the art (relatively vague in the current version). Many sentences in the introduction are too vague such as "some assumptions have been implemented to reconstruct 3D models" (P3L14, which assumptions?) or "A promising reconstruction method … by adapting the DS algorithm. However, large-scale" (P3L16, the "however" refers to something that is not explained, the problem should be clearly stated).

Thank you very much for your constructive suggestions. We rewrote most of the introduction to highlight the specific issues tackled by our paper. Specifically, the history of MPS is compressed in the revised manuscript (see P2L4-L13, L22; P3L4-8); vague descriptions have been corrected (see P3L16-22); and the limitations of the existing have been depicted clearly in the new version (see P2L26-32, P3L25-26, P3L29-34, and P4L1-2).

2. I found the methodology section difficult to follow. Indeed, the proposed approach borrows some techniques from existing algorithms (mostly direct sampling), so that part of the methodology is described in other papers. Although, some parameters are common with DS, the philosophy is quite different as DS is never explicitly calculating cpdf. In that sense, the proposed methodology is closer to classical

approaches such as snesim (except that the cpdf are not stored). I would therefore recommend to explicitly describe every part of the algorithm, without (too many) references to previous publications. Doing so, the methodology would be self-sufficient. Part of the methodology (dissimilarity metrics and MDS) is introduced in the result section and should be moved to the methodology.

We are so sorry for that we did not describe the methodology section clearly. In the revised manuscript, we have reorganized the methodology section. Some existing information but used in the following sections was moved to a new section Background Information, such as the pattern distance (see section 2.1, P5L8-17) and the existing probability aggregation formulas (see section 2.2, P5L18-26 and P6L1-11). The description of dissimilarity metrics and MDS were also move to the section Background Information (see section 2.3, P6L12-17).

3. In the parameter sensitivity, it is argued that some parameters are similar to DS, and thus the paper focuses on the new parameters. Nevertheless, although the proposed method borrow some ideas from DS, it is clear that the approach is different (In DS, you stop searching as soon as you find an occurrence with distance below the threshold, here you continue scanning to get the cpdf). Therefore, we cannot assume without checking that some parameters such as the threshold, the search neighborhood or the fraction of the TI that is investigated will have the same influence in DS and in the proposed approach. In addition, some interaction between the parameters is expected. For example, between the threshold and the maximum number of occurrence, or the number of available sections, some interactions can be expected. Indeed, if you increase the threshold, you will reach faster the maximum number of occurrence.

Thanks a lot for your insightful suggestions. The interaction between two important parameters of DS (distance threshold t and fraction of training image to scan f) and two new parameters presented in our method (number of cross-sections N_{cs} and maximum number of matched patterns from each training image N_{max}) has been added (see section 4.1.4 and Figure 8, P19L5-18 and P20). The results show that these two parameters have similar effects as in DS, so we did not discuss them separately. In addition, it will be repeated with the contents of Meerschman et al. (2013) in which the parameterization of DS was tested thoroughly.

4. The application example is not a real application, but another synthetic benchmark

using a real analog. Indeed, there is no verification data or specific application of the model. I would therefore merge section 3 and 4.

Because section 3 (section 4 in the new version) mainly focuses the parameterization and performance analysis of the proposed method, and section 4 (section 5 in the new version) aims to present a complete example in hydrology, so we kept this section, but changed the title to "Synthetic Example: 3-D Reconstruction of Hydrofacies" in the revised manuscript (see P26L5).

Specific comments:

5. P3L6-25. You don't discuss the paper by Gueting et al. (2017) in the introduction, although it is a recent paper on the topic and you borrow some ideas later in the field example. You should reconsider this paragraph to describe with more details previous approaches and how your method is new.

The description of the paper by Gueting et al. (2017) has been added in the introduction (see P3L32-34 and P4L1-2). In order to clearly explain the problems addressed in our paper, we added detailed descriptions of the limitations of existing methods in the revised version (see P3L25-26, P3L29-34, P4L1-2 and P4L19-23).

6. P4L29-30. This sentence does not necessarily refer to the approach proposed by Comunian et al. (2012), but more globally, to any method assuming stationarity. It is always possible to use auxiliary variable to account for non-stationarity, as it is done by the s2Dcd approach in the application example.

Thanks a lot for pointing it out. We have rewritten the corresponding sentences in the revised version (see P7L3-6).

7. P5L3-8. For reconstruction algorithm, there might be a confusion between training image and hard data. Here, the sections that are used are both training images and hard data. To some extent, using the whole section as TI and the sub-sections as hard data is already a good way to locally constrain the simulations. The s2Dcd algorithm is already performing well in that sense.

The sections that are used in our work are regarded as both training images and hard data, but it is different with s2Dcd. Obviously, s2Dcd uses a series of 2-D simulations to fill a 3-D domain, but a random simulation path containing all uninformed locations is used. The corresponding descriptions have been added in P4L19-22, P7L15-17, and P7L19-21.

8. P5-L9-10. The choice of the subsections within domains is not necessarily selecting the most local information. Indeed, this depends on the location of the node within the subgrid, some other sections might be closer, for example when close to a domain boarder. Since the approach does not store any cpdf, you could center the sub-domain on the node and the TI would change for each node. This would avoid the issue of case 2 in Figure 2, where many nodes closer to the node to simulate are actually out of the TI.

A great idea! But if we adopt this idea, the whole method proposed in this paper has to be changed. In fact, a 3-D domain is divided into several local parts according to the spatial relationship of the cross-sections, and then the MP statistics will be captured from the local surrounding sub-sections for a node to be simulated. This is a very good idea, and we will consider it in our future work.

9. P7L18-20. I am not sure it is intuitive, you might expect that the parallel sections are somehow correlated (except in case of strong non-stationarity), the multiplication of probabilities could then make more sense... and otherwise for perpendicular directions (if the field is highly anisotropic, the orthogonal directions are bringing totally different information)...

Because these two parallel sub-sections often contain similar patterns, and we just expect a larger number of samples and thus more robust pdf by uniting both of them, so we firstly use the additive method to aggregate the parallel ones, then a multiplicative method is used to combine the orthogonal pdfs. In order to depict it more clearly, the corresponding descriptions have been added in P9L15-20.

10. P8L15-18. In short, you compute the cpdf using all the neighborhood whose distances are below the threshold, right?

Yes, we compute the cpdf using patterns whose distances are below the threshold t. But we used a parameter N_{max} to control the number of matched patterns since if this number is large enough, scanning to training images will be not necessary (see P13L1-3 and section 4.1.2).

11. P9L1-3. Multi-grid approach. The description is not clear. How do you divide the data event within several grids? I thought you were selecting all the data and previously simulated nodes within the radius. Are you only considering neighboring nodes that are on the current grid? Or you just mean that for the first grid there are

less points simulated? In practice, everything depends on the radius. Please clarify.

We are so sorry for the unclear description of the multiple-grids used in our work. In the revised version, we added the corresponding description (see P10L24-26). In fact, the neighboring nodes (hard data and previously simulated nodes) around the central node on the current grid are selected to build a data event according to the radius R and the maximum number of points in the neighborhood. Therefore, a large data event is divided into several small parts placed on the different grids which results in smaller neighborhoods on each grid.

12. P9L4-5. I understand that you take the "diagonal nodes" (figure 3) for the smaller grid as they are previously simulated in the multi-grid 2, but the other nodes should also be consider (horizontally and vertically) according to your radius, thus 8 nodes in 2D and 26 nodes in 3D, no? The remark about 3D is strange since you are only considering 3 directions in 2D, this is not a 3D neighborhood or am I missing something? How do you consider previously simulated points or hard data that are out of the 2D planes? Are they simply disregarded, or somehow projected on the plane?

Yes, other nodes will be considered in other two directions. Thank you very much for pointing it out. We have deleted this sentence and added the corresponding description to make it more clear (see P10L29 and P11L2-4). In the local search strategy proposed in this work, three planes through the current simulated node in three orthogonal directions are considered. Other nodes out of the 2D planes will be disregarded (see P11L2-4).

13. P18. Figure 9. The red line shows the proportion in the cross-section, what about the “true” proportion?

The proportions of facies in the 3-D reference have been added and marked by black lines in this Figure in the revised version (see P22L4-6 and Figure 10).

14. P19L6-14. You could actually quantify how realizations are realistic using kernel smoothing (to average the information of the different realizations in a metrics), estimating the density distribution of the realizations around the reference. You can refer to the already cited paper of Hermans et al. (2015) for an application of MDS in the context of 3D MPS in hydrology.

Very useful comment! We have used kernel smoothing to estimate the density

distribution of the realizations of three different MPS approaches around the reference (see P24L1-5). Moreover, the related information about kernel smoothing has been added in section 2.3 in the new version (see P6L18-22).

15. P20L15-16. Still, in DS no cpdf is computed as the first matching sample is selected. Here, you continue scanning, so the effect of those parameters is not necessarily similar. For example, an interaction between t, the number of sections and Nmax is expected.

The interaction between t , f , N_{cs} and N_{max} has been added in the revised version (see section 4.1.4 and Figure 8, P19L5-18 and P20).

16. P22L6. You say that the number of sections is insufficient, but you don't provide guidelines about a sufficient density to use your algorithm. What if the sections are not oriented in orthogonal directions?

A recommended density for the number of sections has been given in P14L18-19. If the sections are not straight or orthogonal, we need to project them in orthogonal directions. The detailed description has been added in the revised manuscript (see P31L6-10 and P32Figure19).

17. P23L2-3. A short description of the auxiliary variable would be welcome. I guess it describes the proportion of facies in the different zones along the vertical direction. It does not have to be long.

A short description of the auxiliary variable has been added in revised manuscript (see P27L6-8).

18. P26L2-3. "partial lower dimensional data" is not true. You can only use 2D orthogonal sections in a sufficient amount. Borehole or analogs cannot be used since you argue that local information is important.

In order to illustrate how partial lower dimensional data are used in our work, we added a figure and the corresponding description in the revised version (see P31L6-10 and P32Figure19).

19. P26L7. But you need a lot of 2D sections, which is a clear drawback of the method.

When there are very few or no sections in a direction, a feasible solution has been suggested by Gueting et al. (2017) where sequential 2D simulations are performed to obtained some sections first, and then both the original informed data and the

obtained sections are used to reconstruct the model of the entire 3-D domain (see P14L19-21).

Technical comments:

20. P12L6-7. Does the "maximum search distance" correspond to the Radius of previous sections?

Thanks a lot for pointing it out! We have used consistent description for this in the revised manuscript (see P14L6 and P21L7)

21. P21L9. You previously mentioned (P17L15) that s2Dcd was using DS with 4 processors. Please check.

It has been corrected in the revised version (see P25L14-19).

22. P23L11. I think it should be Figure 17 instead of 16.

Thank you for pointing it out! It has been corrected in the revised version (see P28L3-4).

Response to Reviewer #3:

This paper presents a locality-based MPS approach to reconstruct 3D geological models based on easily available 2D training images. To fulfil the objective, the MPS search engine roams over only several local sub-sections closer to the simulated node, instead of using a full training image. The authors also perform a parameter sensitivity analysis and the performance comparison with other previous 3D reconstruction techniques, illustrating the effectiveness of their approach using synthetic and real geological data. The results identify better performance both in portraying complex heterogeneous structures and in CPU cost.

All together it is a very good paper, well written and showing a clear and valuable contribution that deserves publication. However, a number of significant issues need to be addressed for this manuscript to be publishable. Therefore, the authors are nevertheless invited to consider carefully the following comments to improve their manuscript.

Thank you very much for your positive and constructive comments and suggestions. We have corrected all the issues you raised in the revised version. The following is a point-by-point response according to your comments.

General comments:

1. I am not totally convinced with the overall contribution of this method compared to s2Dcd. This needs to be explained in detail how the proposed technique differs from s2Dcd, which is now lacking in the introductory part.

We are so sorry for that. We have added some descriptions in the revised manuscript to explain the differences between our method and s2Dcd clearly (see P3L29-32 and P4L19-22).

2. The MDS shows slight improvement in terms of MP simulations using the proposed scheme. The computational benefit only appears with abundant sections available in each direction, which is in practice seldom existing and also mentioned as a limitation in the manuscript. Moreover, the improvement with reproduction of non-stationary patterns might have sampling effect as only one realization is considered from each method.

We used kernel smoothing to estimate the density distribution of the realizations of

three different MPS approaches around the reference (see P24L1-5). The result quantifies the advantages of our approach compared to DS and s2Dcd. Because 4 processors are used in DS and s2Dcd, so our method presents the speedups of about 4 compared to s2Dcd and about 120 compared to DS in this test (see P25L14-19). In addition, if there are very few or no sections in a direction, a feasible solution has been suggested by Gueting et al. (2017) where sequential 2D simulations are performed to obtained some sections first, and then both the original informed data and the obtained sections are used to reconstruct the model of the entire 3-D domain (see P14L19-21). Moreover, we drew the histograms of the four informed segments and the local models of 10 realizations for each MPS method in Figure 18c in the revised manuscript (see P31Figure18c). The result also illustrates the advantages of our approach in reproducing non-stationary patterns (see P30L2-8).

3. Overall, I am struggled to understand the flow of the methodology section, e.g. how the multigrid concept is implemented in searching the neighborhoods, or am I missing something in the workflow of the algorithm? I would also like to see the effects of using various number of multigrid in the form of sensitivity analysis.

We are so sorry for that we did not describe the multiple-grids used in this work clearly. In the revised version, we added the corresponding description (see P10L24-26 and P11L2-4). In fact, the neighboring nodes (hard data and previously simulated nodes) around the central node on the current grid are selected to build a data event according to the radius R and the maximum number of points in the neighborhood. Therefore, a large data event is divided into several small parts placed on the different grids which results in smaller neighborhoods on each grid. Moreover, the effect of the multiple-grids used in this work on computational efficiency is same as the existing ones, so we do not analyze its sensitivity. The main contribution of our strategy focuses on the ability to reproduce features with different scales. It can be observed that our method allows reproducing heterogeneous structures at different scales (see P29Figure17cd).

Specific Comments:

4. P7L2-3: Rewrite the sentence.

This sentence has been rewritten in the revised manuscript (see P16L8-10).

5. P12L12: the connectivity ‘becomes’

It has been corrected in the revised version (see P14L12).

6. P12L14: I would prefer to see an example of artifacts clearly visible on a section of the reconstructed model (maybe with the example of 6x6x6 model in Figure 5), to have the feeling of how bad it is and also to justify the logic behind not using too many cross-sections.

   The first section along X direction of a reconstruction for each case has been added in Figure 5 in the revised manuscript (see P15Figure5). It can be seen that using too many cross-sections will lead to a number of artifacts.

7. P12L18: it 'is' related

   It has been corrected in the revised version (see P14L17).

8. Figure 5: Describe the black and gray lines by adding legend or in figure caption. I think the black lines represent the reference model? Also add the axes labels in variogram and connectivity plots.

   Yes, the black lines represent the corresponding features of the reference models. We have added the descriptions for the black and gray lines and the axes labels in variogram and connectivity plots in the revised manuscript (see P15).

9. P14L8-10: Rewrite the sentence as it's hard to follow in this format.

   This sentence has been rewritten in the revised manuscript (see P16L8-10).

10. P14L14: 120? or 160 or 320?

    Thanks a lot for pointing it out! It should be 160 and has been corrected in the revised version (see P16L14).

11. P17L19: analyze 'the' performance.

    Thank you for pointing it out! We have added "the" before "performance" in P21L15.

12. P17L21: our method

    It has been corrected in the revised version (see P21L17).

13. Figure 8: Caption is incomplete

    The caption of Figure 9 has been corrected in the revised version (see P22L2).

14. Figure 9: The proportions of the facies in the 3D reference could be added as well

in the plot for comparison.

The proportions of facies in the 3-D reference have been added and marked by black lines in this Figure in the revised version (see P22L4-6 and Figure 10).

15. P20L15-16: A brief summary of all other optimized parameters would be helpful for the readers.

A brief summary of all other parameters for computational efficiency has been added in the revised version (see P25L2-4).

16. Figure 13: The figure is redundant as all these numbers are already in the tables.

This figure and the corresponding description have been deleted in the revised version (see P24L14-19, P25L1-2 and P25L6-8).

17. P21L9: s2Dcd uses DS as an external MPS engine as mentioned in P17 L15-16, therefore s2Dcd also runs on 4 processors, I believe. However, the authors claimed the opposite here. Please clarify.

It has been corrected in the revised version (see P25L14-19).

18. P22L6: parts ‘of’ subdomains

It has been corrected in the revised version (see P26L10).

19. P23L5-6: Figure 17 compares the dissimilarity between the sections extracted from the realizations and the informed sections, and I am guessing the sections are selected as random and the authors avoid the sections those are already used as training images?

In fact, all the sections along two directions are exacted, which include both reconstructed sections and informed sections. For each realization, 70 sections (67 reconstructed sections and 3 informed sections) from xz direction and 280 sections (275 reconstructed sections and 5 informed sections) from yz direction are used to draw the MDS maps respectively. The corresponding descriptions have been added in the revised manuscript (see P27L10-14).

20. P23L11: Figure 17 instead of Figure 16.

Thank you for pointing it out! It has been corrected in the revised version (see P28L3-4).

21. P25L1: The segments in Figure 18b are chosen from three local models, so is there

any sampling effect when you select the sections to compare the reproduction of non-stationary patterns? What if you take an ensemble of sections from few realizations to compare the techniques?

Three segments are randomly selected from the three local models. We drew the histograms of the four informed segments and the local models of 10 realizations for each MPS method in Figure 18c in the revised manuscript (see P31Figure18c and P30L2-8). If the surrounding sub-sections of a local area do not contain an attribute but it exists in other locations, the patterns with this attribute will not be moved to this local area in our approach. The corresponding description has been added in P30L2-8.

Locality-based 3-D multiple-point statistics reconstruction using 2-D geological cross-sections

Qiyu Chen [1,2,3], Gregoire Mariethoz [2], Gang Liu [1,3,*], Alessandro Comunian [4], Xiaogang Ma [5]

[1] School of Computer Science, China University of Geosciences, Wuhan 430074, China
[2] Institute of Earth Surface Dynamics, University of Lausanne, 1015 Lausanne, Switzerland
[3] Hubei Key Laboratory of Intelligent Geo-Information Processing, China University of Geosciences, Wuhan 430074, China
[4] Dipartimento di Scienze della Terra "A.Desio", Università degli Studi di Milano, Milan, Italy
[5] Department of Computer Science, University of Idaho, 875 Perimeter Drive MS 1010, Moscow, ID 83844-1010, USA

* *Correspondence to: liugang67@163.com* (G. Liu)

Abstract: Multiple-point statistics (MPS) has shown promise in representing complicated subsurface structures. For a practical three-dimensional (3-D) application, however, one of the critical issues is the difficulty to obtain a credible 3-D training image. However, bidimensional (2-D) training images are often available because established workflows exist to derive 2-D sections from scattered boreholes and/or other samples. In this work, we propose a locality-based MPS approach to reconstruct 3-D geological models on the basis of such 2-D cross-sections, making 3-D training images unnecessary. Only several local training sub-sections closer to the central uninformed node are used in the MPS simulation. The main advantages of this partitioned search strategy are the high computational efficiency and a relaxation of the stationarity assumption. We embed this strategy into a standard MPS framework. Two probability aggregation formulas and their combinations are used to assemble the probability density functions (pdfs) from different sub-sections. Moreover, a novel strategy is adopted to capture more stable pdfs, where the distances between patterns and flexible neighborhoods are integrated on several multiple grids. A series of sensitivity analyses demonstrate the stability of the proposed approach. Several hydrogeological 3-D application examples illustrate the applicability of our approach in reproducing complex geological features. The results, in comparison with previous MPS methods, show better performance in portraying anisotropy characteristics and in CPU cost.

Keywords: Three-dimensional reconstruction, Multiple-point statistics, Locality, Cross-sections, Non-stationarity, Probability aggregation

1. Introduction

3-D characterization of geological architectures plays a crucial role in the quantification of subsurface water, oil and ore resources (*Chen et al.*, 2017; *Foged et al.*, 2014; *Hoffman and Caers*, 2007; *Jackson et al.*, 2015; *Kessler et al.*, 2013; *Raiber et al.*, 2012; *Wambeke and Benndorf*, 2016). Heterogeneity and connectivity of sedimentary reservoirs exert controls on

underground fluid transport (*Gaud et al.*, 2004; *Renard and Allard*, 2013; *Weissmann et al.*, 1999) which is vital to quantify and forecast the formation and distribution of subsurface resources. For a practical 3-D application, however, these attributes are notoriously difficult to characterize and model since the informed data we can acquire are very sparse. Two-point geostatistics (*Goovaerts*, 1998; *Pyrcz and Deutsch*, 2014; *Ritzi*, 2000) and object-based methods (*Deutsch and Tran*, 2002; *Maharaja*, 2008; *Pyrcz et al.*, 2009) are difficult to reproduce anisotropic features and connectivity patterns properly (*Heinz et al.*, 2003; *Klise et al.*, 2009; *Knudby and Carrera*, 2005; *Vassena et al.*, 2010) due to the lack of high-order statistics and the difficulty in parameterization. ~~A variety of two-point geostatistical approaches (*Goovaerts*, 1998; *Journel*, 1993; *Pyrcz and Deutsch*, 2014; *Ritzi*, 2000) have been employed to reproduce 3-D models of subsurface sedimentary structures and facies distribution. Unfortunately, two-point geostatistics cannot capture high-order statistics and hence it cannot properly reproduce anisotropic features and connectivity patterns (*Heinz et al.*, 2003; *Klise et al.*, 2009; *Knudby and Carrera*, 2005; *Lee et al.*, 2007; *Phelps and Boucher*, 2009; *Vassena et al.*, 2010). Object-based methods allow a realistic reconstruction of the heterogeneous lithofacies (*Deutsch and Tran*, 2002; *Maharaja*, 2008; *Pyrcz et al.*, 2009), but it is not always possible to parameterize complicated geological phenomena by a few geometric parameters from irregular data (*Comunian et al.*, 2012).~~ To overcome the abovementioned limitations, multiple-point statistics (MPS) was developed over the recent years and has shown ~~excellent~~ prospects in modeling subsurface anisotropic structures, such as porous media, hydrofacies, reservoir, and other sedimentary structures (~~*Comunian et al.*, 2011;~~ *Dell Arciprete et al.*, 2012; *Hajizadeh et al.*, 2011; *Hu and Chugunova*, 2008; *Oriani et al.*, 2014; *Pirot et al.*, 2015; ~~*Tahmasebi et al.*, 2014;~~ *Wu et al.*, 2006).

A first MPS approach was suggested by *Guardiano and Srivastava* (1993) which is designed to reproduce heterogeneous geometries by extracting spatial patterns from training images directly rather than through variograms. A training image is a conceptual model derived from observations, and it bears a crucial role in MPS-based stochastic simulation. The first efficient implementation of MPS was developed by *Strebelle* (2002) on the basis of a tree structure. ~~Later, the memory-efficient implementation IMPALA based on lists of data events was developed (*Straubhaar et al.*, 2011).~~ Several attempts have thereafter focused on improving MPS algorithms (*Arpat and Caers*, 2007; *Caers*, 2001; *Mariethoz et al.*, 2010; *Straubhaar et al.*, 2011; *Tahmasebi et al.*, 2012; *Wu et al.*, 2008; *Yang et al.*, 2016; *Zhang et al.*, 2006). With these methods, training images are scanned with a fixed search template and the MPS patterns are stored in a tree or a list data structure. ~~For the currently simulated node, the conditional probability density function (cpdf) is calculated according to the current data event.~~ An important difficulty lies in choosing the size of data template to best reproduce large-scale structures (*Strebelle*, 2002). The larger the size of the data event, the fewer replicates of this data event will be found over the training images for inferring the corresponding conditional probability density function (cpdf). However, when the size of data template is too small, large scale structures of the training image cannot be reproduced (*Mariethoz et al.*, 2010). In addition, a search template including too many nodes can lead to storing a large number of patterns, increasing CPU cost and memory consumption. The multiple-grids concept (*Tran*, 1994; *Strebelle*, 2002) mitigates the above-mentioned limitations, but they still present due to the rigidity of data templates and multiple grids. A more straightforward MPS method, Direct Sampling (DS), was proposed by *Mariethoz et al.* (2010) where the high order statistics are sampled directly from the training image

without storing patterns and without the need of multiple grids. One of the main advantages of this approach is that several types of distances between patterns can be considered, making it possible to simulate continuous variables, or even multivariate simulation. As an approximation, pattern distance was used to express the matching degree between the neighborhood of a node and a data event in the training image (*Chugunova and Hu*, 2008; *Mariethoz et al.*, 2010, 2015). ~~For the pdf based MPS methods, using the distances between patterns greatly decreases the amount of stored patterns. Some patch based methods (*Arpat and Caers*, 2007; *Honarkhah and Caers*, 2010; *Tahmasebi et al.*, 2012; *Zhang et al.*, 2006) were proposed on the basis of this concept. By means of computer graphics, two very efficient MPS algorithms (*Li et al.*, 2016; *Mahmud et al.*, 2014) were developed to decrease the computational burden of traditional methods.~~

No matter which MPS algorithm is used, a suitable training image is the fundamental requirement. Although such algorithms are gaining popularity in hydrogeological applications (*Hermans et al.*, 2015; *He et al.*, 2014; *Høyer et al.*, 2017; *Hu and Chugunova*, 2008; *Huysmans et al.*, 2014; *Jha et al.*, 2014; *Mahmud et al.*, 2015), they still suffer from one vital limitation: the lack of training images, especially for 3-D situations. Object-based or process-based techniques are one possibility to build 3-D training images (*de Marsily et al.*, 2005; *de Vries et al.*, 2009; *Feyen and Caers*, 2004; *Maharaja*, 2008; *Pyrcz et al.*, 2009). Besides inherent limitations in the parameterization of these algorithms, it is also challenging to reproduce the various aspects of geological geometries from a high-resolution outcrop map, or even from insufficient borehole data (*Comunian et al.*, 2014; *Pirot et al.*, 2015). To overcome this difficulty of obtaining 3-D training images, scholars have attempted to use low-dimensional data (e.g. boreholes, cross-sections, outcrop and remote sensing images) to reconstruct 3-D models directly instead of a training image in the entire 3-D domain (*Bayer et al.*, 2011; *Comunian et al.*, 2011; *Hu et al.*, 2011; *Weissmann et al.*, 2015). ~~some assumptions have been implemented to reconstruct 3-D models using low-dimensional data (e.g. boreholes, cross-sections, outcrop and remote sensing images) directly instead of a training image in the entire 3-D domain (*Bayer et al.*, 2011; *Comunian et al.*, 2011; *Hu et al.*, 2011; *Weissmann et al.*, 2015).~~ In particular, ~~A promising~~a reconstruction method of partial data sets was proposed by *Mariethoz and Renard* (2010) by using and adapting the DS algorithm. However, large-scale 3-D models contain millions of nodes, thus a very large number of scan attempts will be carried out for each simulated node by using this method, especially in early stages of a simulation due to the sparse known data. Therefore, this method still suffers from a severe computational burden for fine 3-D applications. Moreover, it assumes stationarity of the modeled domain, which is not often the case in practice. *Comunian et al.* (2012) proposed an approach to tackle the lack of a full 3-D training image using sequential 2-D simulations with conditioning data (s2Dcd): a 3-D domain is filled by preserving an overall coherence due to that a series of 2-D simulations performed using 2-D training images along orthogonal directions. However, this strategy is difficult to characterize the connectivity of structures in all directions of a 3-D domain, because each 2-D simulation only considers the high-order statistics in this direction. Moreover, it also suffers from the limitation of nonstationarity of geological phenomena due to the global search in a 2-D plane. To integrate the benefits of the both approaches, *Gueting et al.* (2017) proposed a new combination of the two existing approaches. The combination is achieved by starting with the sequential two-dimensional approach (*Comunian et al.*, 2012), and then switching to the three-dimensional reconstruction approach (*Mariethoz and Renard*, 2010). However, the

above-mentioned limitations of the two approaches still remain because this combination is an optimization of the workflow, and does not substantially improve the methods. To combine the cpdfs from different directions, several probability aggregation methods were tested and discussed (*Allard et al.*, 2012; *Bordley*, 1982; *Genest and Zidek*, 1986; *Journel*, 2002; *Krishnan*, 2008; *Mariethoz et al.*, 2009; Stone, 1961). Other 3-D applications to represent geological structures using MPS and partial data include filling in the shadow zone of a 3-D seismic cube (*Wu et al.*, 2008), generating small scale 3-D models of porous media (*Okabe and Blunt*, 2007) and building a 3-D training image with digital outcrop data (*Pickel et al.*, 2015).

From another perspective, using very common workflows, geologists can obtain 2-D geological maps or sections from scattered boreholes and/or other samples by studying analogs (*Caumon et al.*, 2009). With increasingly sophisticated data acquisition methods, 2-D high-resolution images can be acquired. For example, large-scale outcrop maps can be captured by using terrestrial lidar (*Dai et al.*, 2005; *Heinz et al.*, 2003; *Nichols et al.*, 2011; *Pickel et al.*, 2015; *Zappa et al.*, 2006), and fine-scale pore images can be derived from progressive imaging techniques (*Zhang et al.*, 2010). Therefore, there are many ways to acquire low-dimensional data for reconstructing a full 3-D model. In practice, however, these works using real geological analogs or sections as training images still face significant non-stationarity due to the heterogeneity of geological phenomena and processes (*Comunian*, 2011; *de Vries et al.*, 2009).

To address the insufficient access to a 3-D training image and the challenge of non-stationarity, we present a new strategy to reconstruct 3-D geological heterogeneities using 2-D cross-sections instead of an entire training image. Compared to previous MPS implementations relying on partial data, our proposal is to use only several local sub-sections closer to the simulated node as training images, rather than full planes perpendicular to the *x*, *y* and *z* directions (*Comunian et al.*, 2012) or searching in the entire 3-D domain (*Mariethoz and Renard*, 2010). Against to the filling by a series of 2-D simulations in s2Dcd (*Comunian et al.*, 2012), a random simulation path containing all uninformed locations is used so that MP statistics in a 3-D domain are captured. The local sub-sections are able to offer more coherent and reliable statistics since they are spatially closer to the simulated node which is going to be simulated. Moreover, the original cross-sections are divided into many sub-sections according to their spatial relationships, thus non-stationarity is reduced since it is restricted into a local cube consisting of six or fewer sub-sections. In principle, our proposal can be applied into any multiple-point stochastic simulation method. In this work, we embed this strategy into a standard MPS framework called ENESIM (*Guardiano and Srivastava*, 1993). The blocking strategy proposed in this work can significantly reduce the search space of training images, which makes it possible to get a 3-D reconstruction using ENESIM for a reasonable CPU cost. As with DS, in our method MP statistics are not stored and the neighborhood is flexible. To integrate the patterns from different sub-sections, two probability aggregation formulas and their combinations are used. As an approximation of the matching degree between neighborhoods and data events, pattern distances are used to enhance the stability of cpdfs. Furthermore, we adapt multiple-grids into our approach, where the geometries of data templates are not fixed for grids of different scales. Besides cross-sections, any other scattered samples can also be involved into the proposal as conditional data (hard data).

The remainder of this paper is organized as follows. Section 2 gives background information used in the following sections. Section 3~~2~~ presents the main concepts of the locality-based 3-D MPS reconstruction using 2-D cross-sections and the detailed steps of the proposed approach. Section 4~~3~~ shows a parameter sensitivity analysis and the performance comparison with other MPS algorithms. Section 5~~4~~ gives a synthetic example in hydrogeology~~comprehensive application case~~ to illustrate the effectiveness of our approach when facing the real geological field data. The final section discusses some concluding remarks and ideas for future work.

2. Background Information

2.1. Pattern Distance

A pattern distance $d\{\mathbf{N}_X, \mathbf{N}_Y\}$ is an approximation of the dissimilarity between patterns, which is used to compare the neighborhood of a node currently simulated with a data event in the training image (*Mariethoz et al.*, 2010). Approximate matches are accepted by using a distance threshold t. Namely for a data event $\mathbf{N}_X$ from the simulation grid, when the condition $d\{\mathbf{N}_X, \mathbf{N}_Y\} \le t \ \ (t \ge 0)$ is met, the pattern $\mathbf{N}_Y$ from the training image will be used to update the current cpdf. For a categorical variable, the distance can be formulated as:

$$d\{\mathbf{N}_X, \mathbf{N}_Y\} = \frac{1}{n}\sum_{i=1}^{n} a_i \in [0,1], \qquad where \ \ a_i = \begin{cases} 0 & \text{if } Z(x_i) = Z(y_i), \\ 1 & \text{if } Z(x_i) \ne Z(y_i). \end{cases} \tag{1}$$

For a non-stationary training image from an actual geological phenomenon, repeatability of spatial patterns could be weak so that it is hard to acquire a stable cpdf. Therefore, we adopt a patterns distance with a threshold as an approximation to sample more patterns and get a more stable cpdf.

2.2. Probability Aggregation

Allard et al. (2012) presented a comprehensive literature review for aggregating probability distributions. These can be divided into additive methods and multiplicative methods according to their mathematical properties. Linear Pooling formula (*Stone*, 1961) is a widely used method (for example, it was used by *Okabe and Blunt*, 2007) based on the addition of probabilities. It is appealing because of its flexibility and simplicity. Multiplicative methods include Bordley/Tau models and log-linear pooling (based on odd ratios) (*Bordley*, 1982; *Journel*, 2002; *Genest and Zidek*, 1986).

2.2.1. Linear Pooling Formula

The linear pooling formula, proposed by *Stone* (1961), probably is the most intuitive way of aggregating the probabilities $P_1, ..., P_n$ of an event A.

$$P_G(A) = \sum_{i=1}^{n} w_i P_i(A) \quad \text{with } w_1,...,w_n \in \mathbf{R}^+. \tag{2}$$

In this formula, w_i are positive weights and their sum must equal one to obtain a global probability $P_G \in [0,1]$.

2.2.2. Log-Linear Pooling Formula

The~~A~~ log-linear pooling ~~operator~~ formula is a linear operator of the logarithms of the probabilities (*Genest and Zidek*, 1986). If a prior probability $P_0(A)$ must be included, ~~the log-linear pooling formula~~it is written as:

$$P_G(A) \propto P_0(A)^{1-\sum_{i=1}^{n} w_i} \prod_{i=1}^{n} P_i(A)^{w_i}. \tag{3}$$

$\sum_{i=0}^{n} w_i = 1$ is needed to verify external Bayesianity. There are no other constraints whatsoever on the weights w_i, $i = 0,...,n$. The sum $S = \sum_{i=1}^{n} w_i$ plays an important role in this formula. If $S = 1$, the prior probability P_0 is filtered out because $w_0 = 0$. Otherwise, if $S > 1$, the prior probability has a negative weight and P_G is further away from P_0 than other probabilities. Conversely, if $S < 1$, P_G is always closer to P_0. Therefore, we can adjust the influence of the prior probability P_0 on the aggregated result P_G by changing the value of S.

2.3. Multidimensional Scaling and Kernel Smoothing

Tan et al. (2014) proposed a distance-based approach to evaluate the quality of MP simulation outcomes where the Jensen–Shannon (JS) divergence is used to depict the dissimilarity of MP histograms as a quantitative metric. The information in the dissimilarity of MP histograms can be visualized using multidimensional scaling (MDS) (*Caers*, 2011). MDS approximates these distances by a lower-dimensional Euclidean distance in Cartesian space, which facilitates the visualization of the dissimilarity of MP histograms.

Hermans et al. (2015) used an adaptive kernel smoothing (see *Park et al.*, 2013) to estimate the probability density of the data variable for each kind of realizations $f(\mathbf{Ref}^*|\mathbf{R}_i)$ in the *d*-dimension space inferred from MDS. This allows estimating the probability density distribution of the realizations around the reference. For each kind of realizations, its probability relative to the reference $P(\mathbf{R}_i|\mathbf{Ref})$ can be calculated by using Bayes' rule:

$$P(\mathbf{R}_i|\mathbf{Ref}) \approx P(\mathbf{R}_i|\mathbf{Ref}^*) = \frac{f(\mathbf{Ref}^*|\mathbf{R}_i)P(\mathbf{R}_i)}{\sum_{i=1}^{N} f(\mathbf{Ref}^*|\mathbf{R}_i)P(\mathbf{R}_i)}. \tag{4}$$

3. Methodology

3.1. Local Search Strategy of 3-D MPS Reconstruction

In the above-mentioned MPS methods using partial data whether searching an entire 3-D domain or complete sections, ~~*Comunian et al.* (2012) presented a commonly used 3-D MP simulation approach using 2-D training images. The key idea is to capture 3-D MP statistics by using two/three orthogonal training images and then merging the MP statistics from different directions into an integrated pdf. However,~~ any locations of the training images are scanned even they are far away from the simulated node so that one spatial pattern will be carried to a distant position. Therefore, the use of these~~is~~ methods is~~is~~ restricted to stationary training images, which are in practice seldom available. In this work, we propose a local search strategy that allows palliating this problem, by taking into account the spatial relationships of the real geological cross-sections in a given 3-D domain.

As illustrated in Figure 1, a 3-D domain is segmented into nine small blocks by six cross-sections from three orthogonal directions where there are two sections in each direction. Every local block is surrounded by n local sub-sections ($1 \le n \le 6$). It should be noted that, sometimes, local blocks are not closed (i.e. the surrounding sub-sections are less than six) (Figure 1b); and it is also allowed sections along some planes are missing; however, at least one section should be provided. For each unknown node in the local block (e.g. the gray cubes in Figure 1c), the MP statistics are captured from the surrounding sub-sections rather than from the entire sections. Namely, there are n corresponding training images for each simulated node. These local sub-sections are the parts of the global cross-sections which are closer to the uninformed nodes in the local block, thus they are more likely to be regarded as statistically representative. Data events are selected from the informed nodes (hard data) on three planes parallel to the sub-sections and through the current simulated node in three orthogonal directions by using a flexible neighborhood.

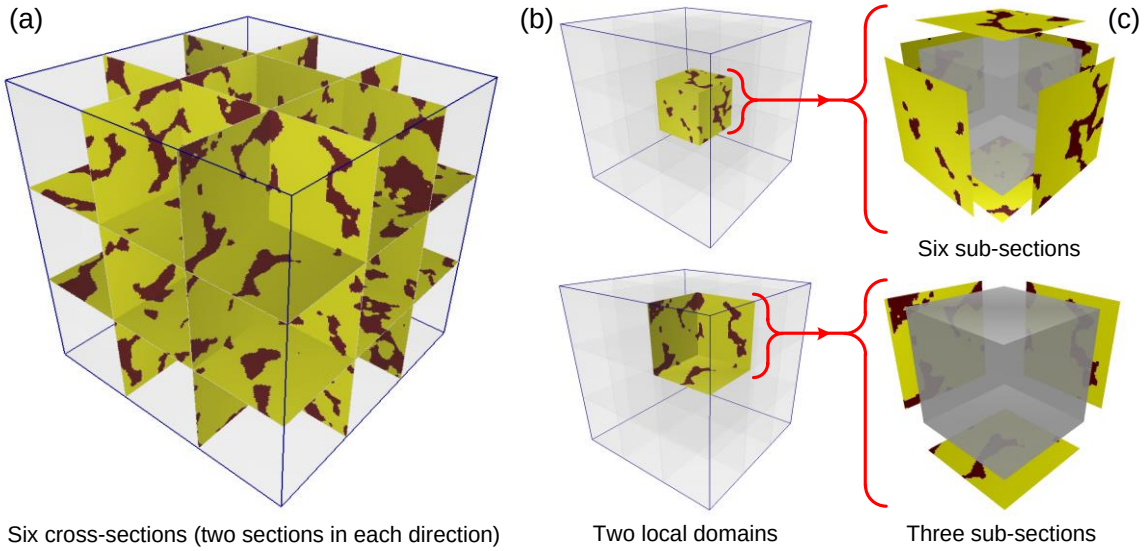

Figure 1. Local sub-sections divided by their spatial relationships and the corresponding training images. (a) Six cross-sections in a 3-D domain: two sections along each direction; (b) two local domains: a central cube and a corner cube; (c) corresponding sub-sections (training images).

Another important point is related to handling of the search window when scanning a sub-section. Here, we allow all locations of a sub-section to be visited by the central node of a data event. The neighbor nodes of the data event can be placed in other adjacent sub-sections when matching with the training images. As shown in Figure 2, the area inside the blue line is the search window. If only the nodes of the data event are from the sub-section itself (case 1 on the figure), the training patterns are seriously reduced. We adopt a search strategy where neighbor nodes can be searched in the neighboring sub-sections (case 2 on the figure). Its main advantages are the coherence of the spatial patterns in a realization and the larger number of training patterns available. In addition, the size of the data events is constrained by the boundary of the global section, as illustrated in *Mariethoz et al.* (2010).

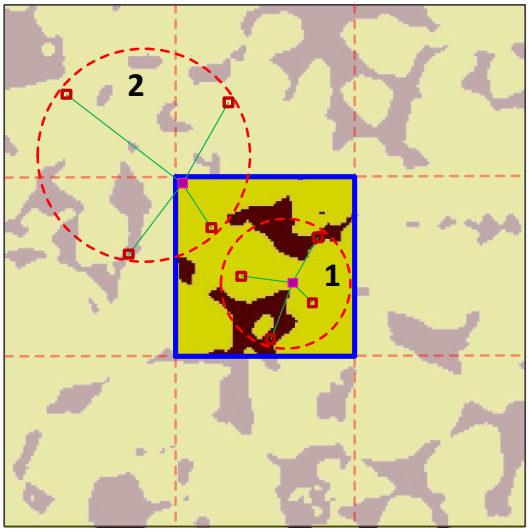

Figure 2. Search window in sub-sections.

If more cross-sections are available, a finer spatial subdivision can be used. In this case, the size of each sub-section is smaller and the computational cost is reduced significantly. However, extremely small training images cannot offer enough spatial patterns, thus a minimal sub-section size has to be considered. In practice, if there are many sections in each direction, a feasible solution is to select several ones as the references and others are used as conditioning data only.

3.2. Strategy for Aggregating the pdfs from Local Sub-Sections

As an additive aggregation method, the linear pooling formula corresponds to a mixture model, which is related to the union of events and to the logical operator OR (*Allard et al.*, 2012). This method is thus used to unite several independent probabilities into a global term P_G. The log-linear pooling formula, based on the multiplication of probabilities, is related to the intersection of events and to the logical operator AND. Therefore, we usually use such a method to aggregate the probabilities with significant correlation to acquire a conjunction probability.

In this study, n pdfs ($1 \le n \le 6$) are computed from the surrounding local sub-sections (Figure 1). For the illustrative case proposed here, a local 3-D domain is surrounded by six sub-sections, and six pdfs are being aggregated. There are two parallel sub-sections (training images) in each direction. ~~Intuitively, an~~ An additive aggregation operator ~~seems~~ is more appropriate to combine such two disjunctive probability distributions, since these two parallel sub-sections often contain similar patterns, and we just expect a larger number of samples and thus more robust pdf by uniting both. Then, three orthogonal pdfs are obtained. We then join these pdfs containing the statistics from different directions with obvious anisotropic features. This scenario needs a multiplicative method to combine the orthogonal pdfs so as to retain the features in all directions. In summary, an optimal probability aggregation strategy is proposed by the procedure described below:

1. Aggregate the pdfs collected along the same direction for parallel sub-sections using the linear pooling formula described in section 2.2.1.

2. Aggregate the orthogonal pdfs from the above step by using the log-linear pooling formula described in section 2.2.2.

Of course, the probability aggregation step is not required when for step 1 there is only one sub-section along a given plane, and for step 2 the pdf that along some direction are missing are simply not included in the aggregation process. For the step 1, the weights w_1 and w_2 are related to the distances between the current location and the two parallel sub-sections d_1 and d_2 s, and computed as:

$$w_1 = \frac{1/d_1}{1/d_1 + 1/d_2}, \; w_2 = \frac{1/d_2}{1/d_1 + 1/d_2}. \quad (35)$$

Such parameterization ensures that within-block trends are accounted for.

For the step 2, an influence of the prior probability is desired to tune the other orthogonal pdfs. Thus, we usually use $0 < w_0 < 1$, and set $w_i (i = 1, ..., n)$ equal, i.e. $w_i = (1 - w_0)/n$, where n is the number of pdfs to be aggregated. However, the weights $w_i (i = 1, ..., n)$ can also change, for example, they can vary at each simulation step as described in *Comunian et al.* (2012), according to the contributions of the different training images, while sum still respects the condition $\sum_{i=0}^{n} w_i = 1$.

3.3. Flexible Search Template on Multiple Grids

When large neighborhoods are considered, it is more difficult to find matching data events in the training image and thus a larger distance threshold t is required to obtain a sufficient number of samples for an acceptable cpdf. This can lead to degrading small-scale features or the removal of categories that have a low proportion. To address this issue, we propose a novel implementation of multiple grids where the search template is flexible and the distance threshold t varies according to the radius of the neighborhood.

As illustrated in Figure 3, an example of multiple grids with three levels is used to show the relationship between neighborhoods, search radius R and distance threshold t on different grids. A neighborhood is identified by the informed and/or simulated nodes located in the circle with a radius R and the current node (the gray nodes in Figure 3) as a central. The initial radius R_0 and distance threshold t_0 for the first grid are assigned as the input parameters. The radius R linearly reduces to 1 from the first to the last grid, and the threshold t similarly varies from 1 to 0. The neighboring nodes (hard data and previously simulated nodes) around the central node on the current grid are selected to build a data event according to the radius R and the maximum number of points in the neighborhood. Therefore, a~~A~~ large data event is divided into several small parts placed on the different grids which results in smaller neighborhoods on each grid. An acceptable threshold t is thus assigned to each neighborhood. For the last grid, the radius is reduced to 1 and at most there are eight nodes in a neighborhood ~~(Figure 3 is a 2-D sketch of multiple grids, but we mainly focus on 3-D simulations in this paper)~~. This

strategy considers that small data events located on the last grid are much more repetitive (thus easier to find) than the large data events of the first grid. Figure 3 shows the flexible use of multiple grids on one plan through the current node. In the local search strategy proposed in this work, three planes through the current simulated node in three orthogonal directions are considered. Thus the same strategy will be applied on other two planes.

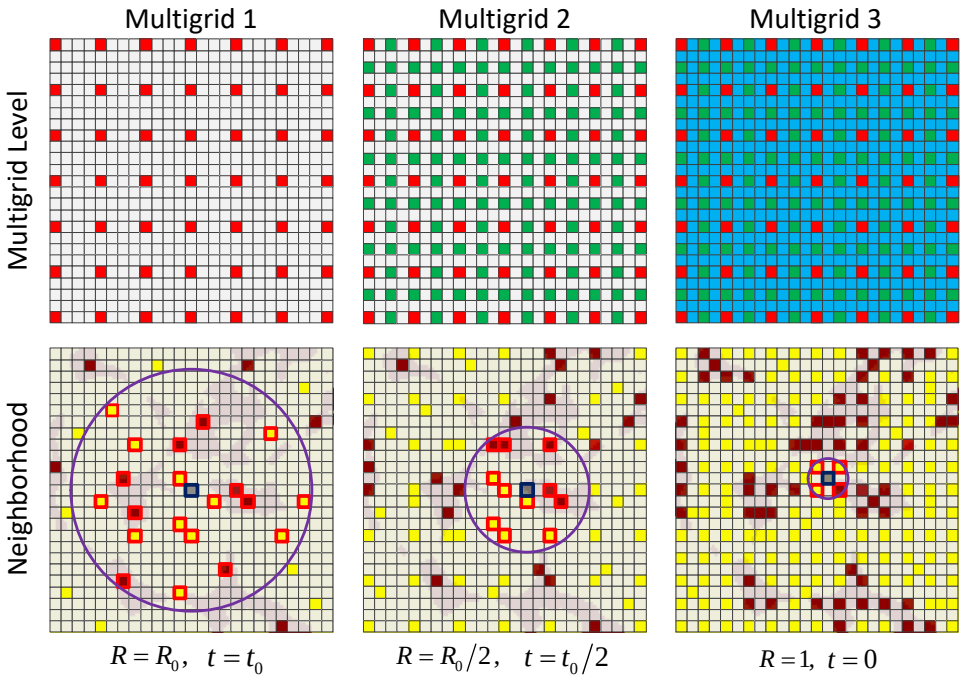

Figure 3: An example of multiple grids and the corresponding neighborhoods, search radius R and distance threshold t.

3.4. Step-by-Step Algorithm Using the Local Search Strategy

Based on the strategies proposed in the above sections, the detailed steps of our simulation algorithm proceed as illustrated in Algorithm 1.

Algorithm 1: Reconstruct 3-D geological structures using 2-D cross-sections

1 Load data files, assign all points of the training data (cross-sections and other samples) into the SG.
2 Record the indexes of the sections in *x*, *y*, *z* directions and compute the prior proportions $\mathbf{P}_p$ of the local domains.
3 **For** each multiple grid g :
4 Define a random simulation path for grid g according to the remaining nodes.
5 **Do** until all uninformed nodes in g have been visited:
6 Get the index of current node $\mathbf{x}$, and identify its neighborhood $\mathbf{N}_x$.
7 Obtain the indexes of the closest sections around $\mathbf{x}$: $\{x_0, x_1\}$, $\{y_0, y_1\}$, $\{z_0, z_1\}$.
8 Randomly scan the sub-sections (TIs) and get the corresponding cpdfs (see algorithm 2).

9 Get the prior proportion $\mathbf{p}$ of the local domain according to the location of the node $\mathbf{x}$.

10 Combine the cpdfs and $\mathbf{p}$ into a joint pdf using the strategy presented in section 3~~2~~.2.

11 Randomly draw a value from the final pdf, and assign it to location $\mathbf{x}$.

12 **End**

13 **End**

As mentioned above, we capture the MP statistics from several sub-sections of a local domain. Thus, the corresponding prior proportion should also be computed on the basis of these surrounding sub-sections (step 2). Obviously, step 8 is the most important procedure in our simulation algorithm, and the idea is inspired from ENESIM (*Guardiano and Srivastava*, 1993) and DS (*Mariethoz et al.*, 2010). The main procedure is demonstrated in Algorithm 2.

Algorithm 2: Scan a local sub-section (training image) in one certain direction

Input: $\mathbf{x}$**:** current simulation location; id : index of the training image that will be scanned;

$\chi_0, \chi_1, \gamma_0, \gamma_1$: indexes of the closest training image s in the other two directions.

Output: cpdf: conditional probability density function from the current training image.

1 **Function** ScanTI($\mathbf{N}_x, id, \chi_0, \chi_1, \gamma_0, \gamma_1, \&\text{cpdf}$)

2 Get the sub-section sub_S (training image) according to the id and $\chi_0, \chi_1, \gamma_0, \gamma_1$;

3 Set a random path p, and initialize the counter of matched patterns $sum = 0$;

4 **for** $i := 0 \rightarrow p.\text{size}()$ **such that** $i < p.\text{size}() \times f$ **do**

5 Sample a location in the training image and get the neighborhood $\mathbf{N_Y}$;

6 Compute the distance $d\{\mathbf{N_X}, \mathbf{N_Y}\}$ using equation (~~4~~1) presented in section 2.1;

7 **if** $d\{\mathbf{N_X}, \mathbf{N_Y}\} \le t$ **then**

8 update the cpdf according to the facies of the central point in the training image;

9 $sum{+}{+}$;

10 **end if**

11 **if** $sum > N_{\max}$ **then**

12 **break;**

13 **end if**

14 **end for**

15 **end Function**

The fraction of the scanned training image f and the distance threshold t are borrowed from DS and they play the same roles. $\chi_0, \chi_1, \gamma_0, \gamma_1$ are the indexes of the closest training images in the other two directions and they are used to

determine the current sub-section (training image). A new parameter, the maximum number of matched patterns from the training image N_{max} is adopted to avoid unnecessary searches. For some small neighborhoods, especially in the last multiple grid, the cpdf will rapidly stabilize with the increasing number of matched patterns.

4. Parameterization and Performance Analysis

In this section, we apply our method on several synthetic cases where the cross-sections are extracted from existing 3-D references. Using these examples, we perform a parameter sensitivity analysis and compare it with two widely used methods, DS-based 3-D reconstruction (*Mariethoz* and *Renard*, 2010) and s2Dcd (*Comunian et al.*, 2012). The workflows and algorithms proposed in this work are developed in the C++ programming language. All experiments presented in this paper are implemented on a laptop computer with Intel 4-Cores i5-62000U Quad-core CPU 2.30 GHz, 8 GB RAM and 64 bit Windows 10.

4.1. Parameter Sensitivity

The majority of parameters of our approach are similar to DS. Therefore, only the sensitivity of three parameters specific to our approach are tested against the 3-D reference shown in Figure 4, considering CPU cost and statistical and geometrical features of the realizations obtained. All cross-sections used in the following tests in the section 43.1 are extracted from this 3-D model.

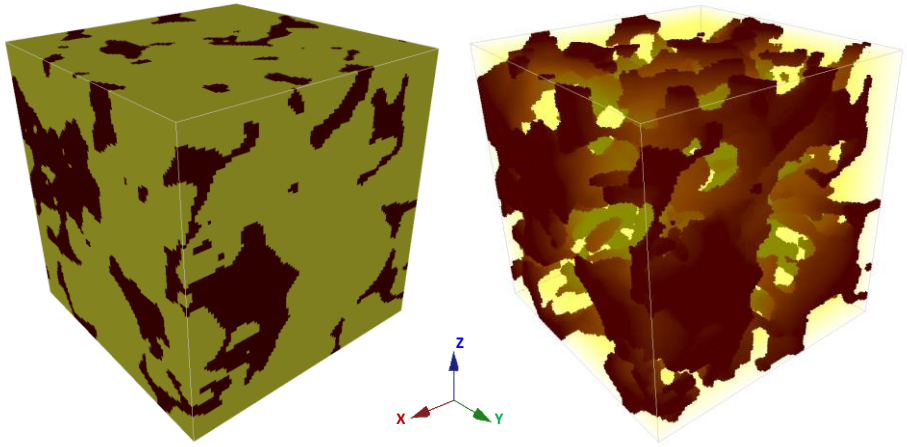

Figure 4. A sample of Berea sandstone from *Okabe and Blunt* (2007) is used as a 3-D reference (100 × 100 × 100 voxels). The crimson color represents pores and the yellow color represents matrix. The porosity of this model is 20.33%.

4.1.1. Number of Cross-Sections

The number of cross-sections N_{cs} is a new parameter in our approach. They are not only regarded as the training images and conditioning data, but also control the computing speed and the quality of the reconstructions. Figure 5 and Table 1 show different reconstructions and their statistical properties by increasing the sections in every direction. In this test, the number of cross-sections N_{cs} in each direction increases from one to six, and other parameters are fixed: maximum search ~~distance~~ radius = 50, maximum number of points in a neighborhood = 35, distance threshold $t_0 = 0.2$, fraction of training image to scan $f = 0.8$, maximum of matched patterns from each training image = 100, number of multiple grids = 3, weights of the probability aggregation $w_0 = w_1 = w_2 = w_3 = 0.25$. We obtain 20 realizations for each set of cross-sections. The main difference between the different settings is the improvement of computational efficiency with the increase in cross-sections. The proportion of pores (porosity) is reproduced at a similar level for each group, Also, when increasing the number of cross-sections N_{cs}, the number of geobodies gets closer to the reference, and the variability is decreased and the connectivity ~~is more and more~~ becomes stable, which are caused by the increase of conditioning data (i.e. informed cross-sections). On the other hand, using too many cross-sections will lead to a number of artifacts since the training sub-sections for each sub-block are very small, resulting in insufficient number of samples (see the sections extracted from the reconstructions in Figure 5). As a consequence, we recommend that several sections can be chosen if there are abundant candidates in one direction, which must ensure that the features of selected ones are diverse and contain enough spatial patterns, but not incurring artifacts. In this test, 3 or 4 sections in each direction are recommended, but it is related to the size of simulation grid in other 3-D application. In general, one informed section for every 50 grid cells in one direction in the simulation grid is recommended. When there are very few or no sections in a direction, a feasible solution has been suggested by *Gueting et al.* (2017) where sequential 2D simulations are performed to obtained some sections first, and then both the original informed data and the obtained sections are used to reconstruct the model of the entire 3-D domain.

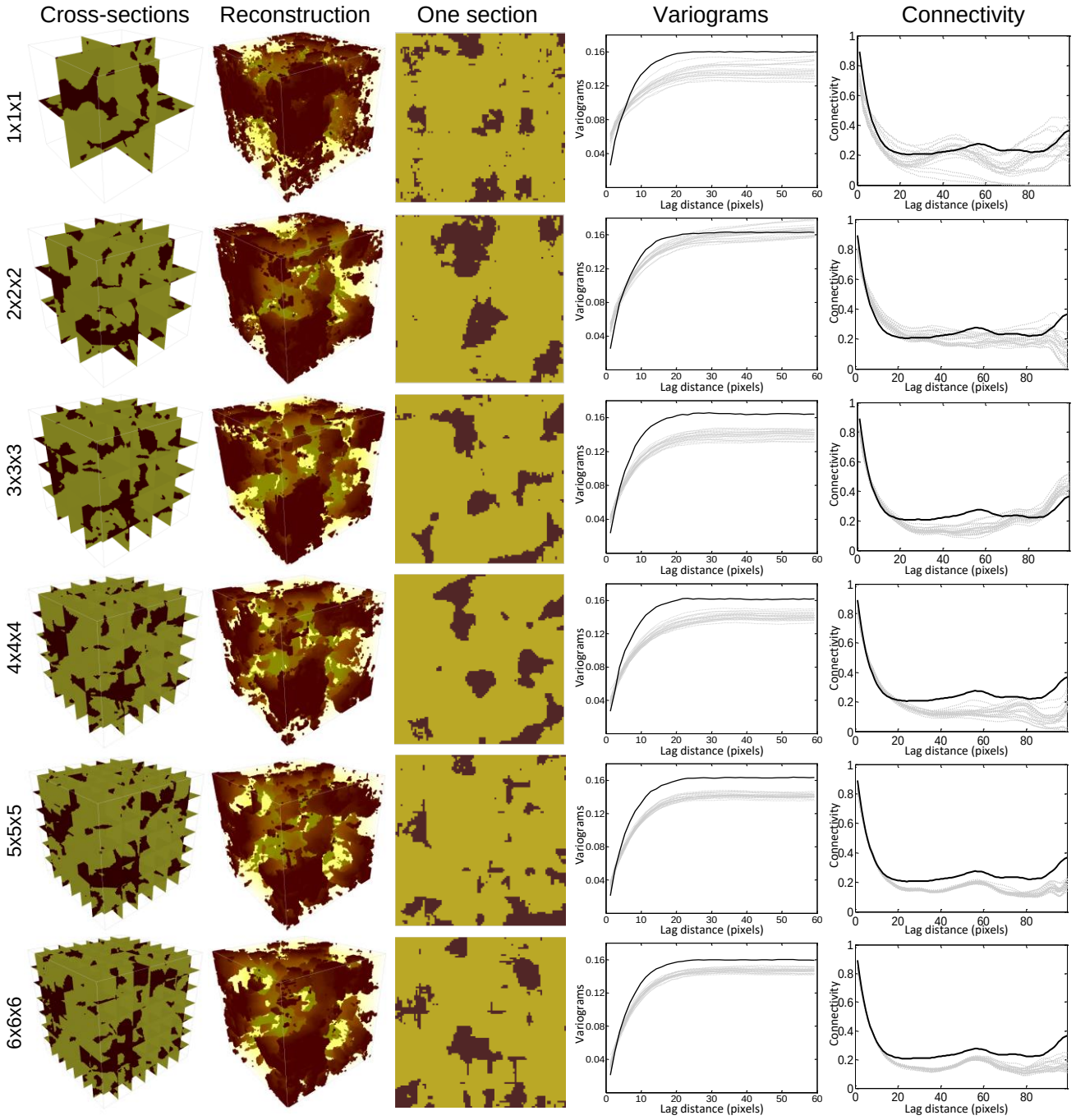

Figure 5. Reconstructions and their statistical properties with increasing the number of sections in each direction. The first section along X direction of a reconstruction for each case is presented here. We only present the connectivity functions computed along the coordinate Y since their features are similar in three directions. The black lines represent the corresponding features of the reference models, and the gray lines represent the features of the reconstructions.

Table 1. Comparison of the performance of the tests in Figure 5. All the statistics are the averages of 20 realizations.

Test	N_{cs}	Sub-blocks	Porosity (%)		No. of geobodies	Time (s)
			Training sections	Results		
1×1×1	3	8	19.07	16.36	1781	1382
2×2×2	6	27	21.35	19.95	908	718
3×3×3	9	64	18.70	16.22	572	396
4×4×4	12	125	19.62	16.21	471	271
5×5×5	15	216	19.81	16.80	340	183
6×6×6	18	343	19.74	17.32	326	127
3-D Ref.			**20.33**		**144**	

4.1.2. Maximum Number of Matched Patterns from Each Training Image

Table 2 shows the statistics of 20 realizations obtained by varying the maximum of matched patterns from each training image N_{max}, which is a novel parameter adopted in this work to avoid the unnecessary searches during obtaining a cpdf from training images. Other parameters are the same as in the former test presented in Figure 5, except for the sections in each direction which are fixed to 3. We find that the computational cost increases sharply when N_{max} >160 and then stabilizes. Concerning the compared statistical properties, low values of N_{max} result in variabilities ~~are closer to the reference with bigger variances which is due to~~ because it is almost like sampling the result directly from training images ~~resulting in~~and the role of cpdfs is lost. For the remaining cases, the statistics are similar except for a decrease of variances with increasing N_{max} (Table 2). In order to better grasp the effect of N_{max}, three cases are selected (N_{max} = 5, 40, 320) and the corresponding realizations are shown in Figure 6a-c. The connectivity functions vary in a large range for small N_{max} values. Conversely, they become more stable when increasing N_{max} (Figure 6d). The variance of variables bears the same tendency by increasing N_{max} (Figure 6e). Consequently, N_{max} = 40 to ~~120~~ 160 is recommended resulting in a balance between a stable cpdf and computational cost.

Table 2. Comparison of the performance for 20 realizations with three sections in each direction, and varying the maximum of matched patterns from each training image N_{max}. Other parameters are fixed and are same with the test of Figure 5. All the statistical values are the mean of 20 realizations. ∞ represents no constraint for N_{max}.

N_{max}	Porosity (%)	Variance	No. of geobodies	Time (s)
5	18.39	0.150	365	132
10	17.22	0.143	440	161
20	16.69	0.139	486	200
40	16.47	0.138	505	251
80	16.48	0.138	510	417
160	16.38	0.137	519	495
320	16.50	0.138	503	549
640	16.66	0.139	508	587
∞	16.89	0.138	497	589
Ref.	**18.70**	**0.152**	**144**	

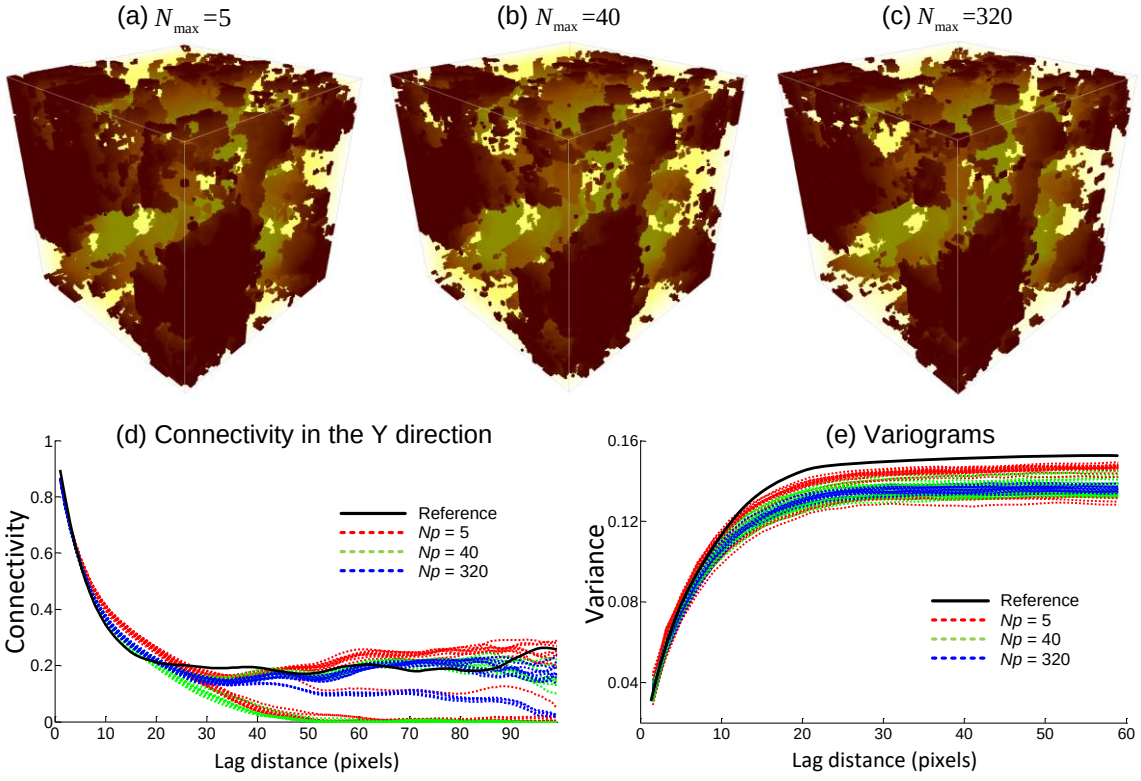

Figure 6. Reconstructions and their statistical properties with N_{max} = 5, 40, 320 selected from Table 2.

4.1.3. Weights of the Probability Aggregation Formulas

In this work, the strategy for aggregating the pdfs from local sub-sections includes two steps. In the first step the weights of Linear Pooling Formula for two parallel sub-sections are selected depending on the distances between the current location and the two sub-sections in the first step. Therefore, the weights are automatically set and do not need to be set. In the second step, the appropriate weights for the prior probability distribution and three orthogonal cpdfs are to be selected by the user. Figure 7 shows different realizations obtained by varying the four weights w_0, w_1, w_2, w_3. Here we increase the weight of the prior probability distribution w_0 and let the other three weights equal, since the cpdfs from three orthogonal directions have the same contribution. Of course, if users think the cpdf of one direction is more important than others, they can be changed, under the constraint that $\sum_{i=0}^{3} w_i = 1$. It can be observed that when $w_0 = 0$, the spatial structures are well reproduced, but with larger variance (Figure 7a) since all spatial patterns are inferred from the MP statistics of the surrounding sub-sections rather than using prior information. When increasing w_0, the ~~continuity~~ connectivity of the spatial structures is degraded, but the facies proportions are closer to the reference (Figure 7b). Finally, in the extreme case of (Figure 7c) the connectivity ~~continuity~~ of spatial structures is lost. Therefore, $0 \le w_0 \le 0.25$ is a recommended range and other three weights can be determined by the importance (e.g. complexity or variety of patterns) of the sections in each direction.

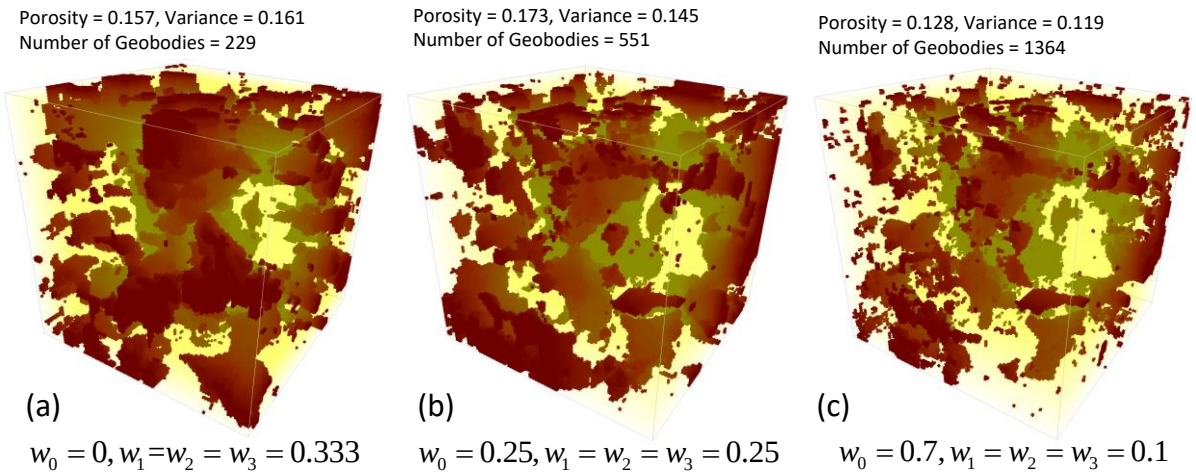

Figure 7. Three realizations obtained by varying the weights of the probability aggregation formulas. Three sections in each direction are used and other parameters are same with the test of Figure 5.

For the other parameters involved in our algorithm, most of them are similar to the parameterization of DS which have been tested thoroughly in *Meerschman et al*. (2013). However, our method allows larger initial values for the neighborhood size and the distance threshold because multiple grids are used so that these initial values are decreased with increasing the level of multiple grids.

4.1.4. Interaction between t, f, N_{cs} and N_{max}

In this section, we compare the interaction between two important parameters of DS (distance threshold t and fraction of training image to scan f) and two new parameters presented in our method (number of cross-sections N_{cs} and maximum number of matched patterns from each training image N_{max}). Figure 8 shows the interaction between t, f, N_{cs}, N_{max}. Running our algorithm with $f = 0.2$ and $t = 0.4$ results in noisy realizations. This is not surprising since any patterns can be accepted even if it bears a large pattern distance $d\{\mathbf{N}_X, \mathbf{N}_Y\}$. Of course, the algorithm will be very fast under these parameters because the scan for training image will be stopped at the beginning. *Meerschman et al*. (2013) tested thoroughly for the parameterization of DS. In their test, when $f = 0.5$ and $t = 0.2$, the realizations are acceptable. However, here the results still contain many noises since the local search strategy reduces the size of the actually scanned training images. As the increase of t, f, N_{cs} and N_{max}, the results become satisfactory. The recommended range of N_{cs} and N_{max} have been given in the above sections. In our method, it is advised to use $f \geq 0.8$ and $t \leq 0.1$. Compared to DS, more strictly restrictions for t and f are adopted due to the local search strategy used in our method. Same as the effect of t and f, N_{cs} and N_{max} also control the computational efficiency and the quality of simulations. Therefore, when setting the parameters, we should consider finding a balance between the quality of results and the computational cost.

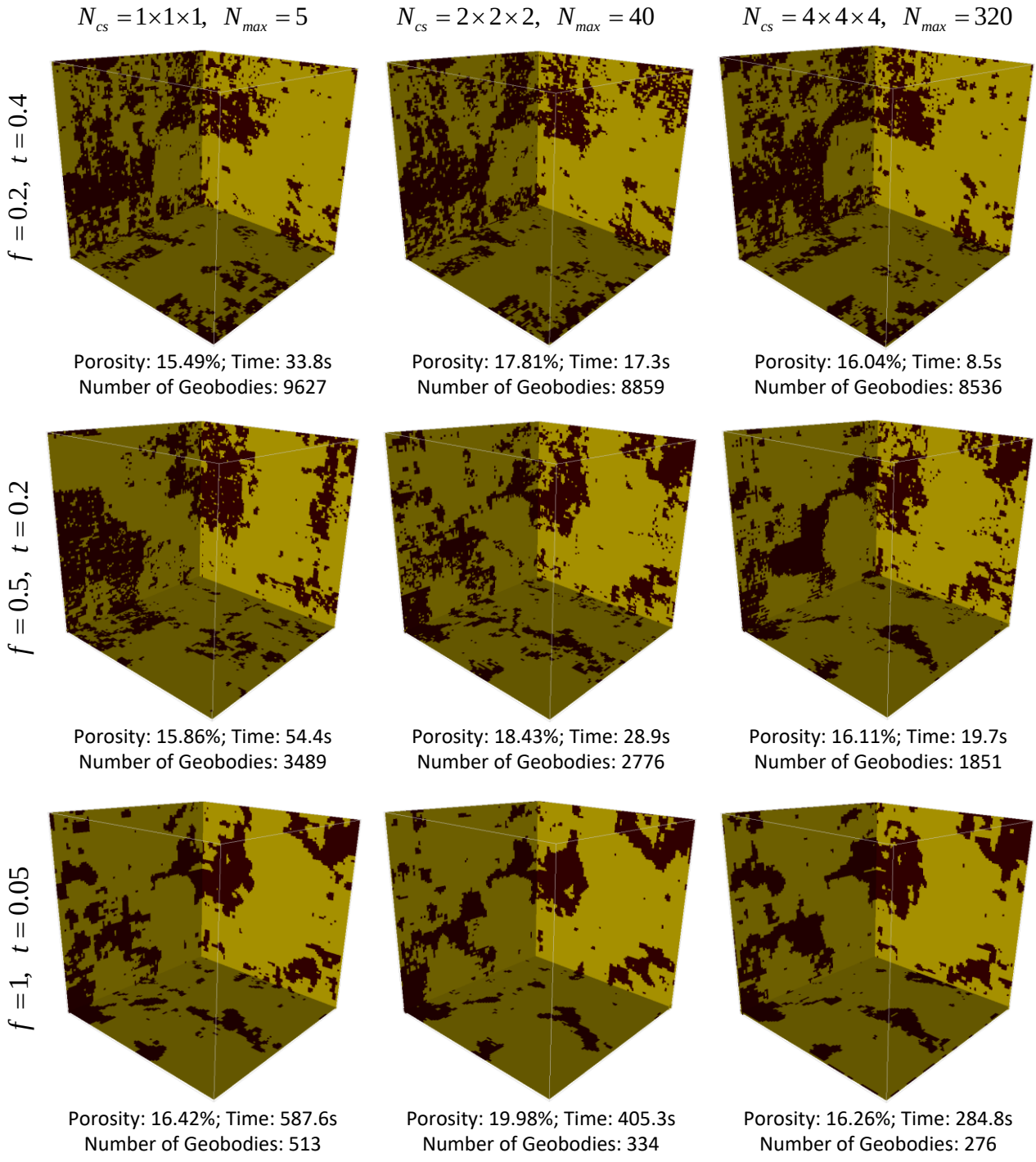

Figure 8. Interaction between t, f, N_{cs} and N_{max}. These first sections in three directions of each realization are presented. The porosity, CPU time and the number of geobodies are the average of 10 realizations.

4.2. Comparison of Reproducing Heterogeneities with Existing Methods

To verify the validity of our approach for reproducing heterogeneous structures, we compare it with two MPS implementations that use partial data: DS (*Mariethoz and Renard*, 2010) and s2Dcd (*Comunian et al.*, 2012). As shown in Figure 98, six cross-sections extracted from a 3-D model of folds (180 ×150 × 120 voxels) (*Mariethoz and Kelly*, 2011) are utilized in this test. s2Dcd is a wrapper library that requires an external MPS engine. In order to ensure comparability, here DS is employed as the engine of s2Dcd. The detailed parameters are as follows: maximum search ~~distance~~ radius = 40, maximum number of points in a neighborhood = 40, distance threshold $t_0 = 0.2$, fraction of training image to scan $f = 0.8$, maximum of matched patterns from each training image = 100, level of multiple grids = 3, weights of the probability aggregation $w_0 = w_1 = w_2 = w_3 = 0.25$. In other two methods, a smaller distance threshold $t = 0.05$ is considered and other essential parameters are same with our method. Because the implementation of DS is parallel, we use 4 processors to carry out this test in DS and s2Dcd. Only one processor is used in our method because our implementation is not parallel. In Figure 98, one selected realization for each method is presented. From their visual appearance, it looks that s2Dcd and our method have the similar performance for reproducing the patterns shown in 3-D reference and informed cross-sections. Therefore, histograms, variograms, and connectivity functions are used to further analyze the performance. Figure 109 shows the comparison of proportions of the facies for the realizations by using three MPS methods. 20 realizations are performed for each method. It can be seen that the facies proportions with our method~~s~~ are closer to the proportions of the reference model and the informed cross-sections. The variograms and the connectivity functions on three directions for the 3-D reference and the generated 20 realizations of each method are shown in Figures 1110 and 1211, indicating that all three methods are able to reproduce the basic statistics of the 3-D reference, but the lines of the proposed method are generally closer to the reference.

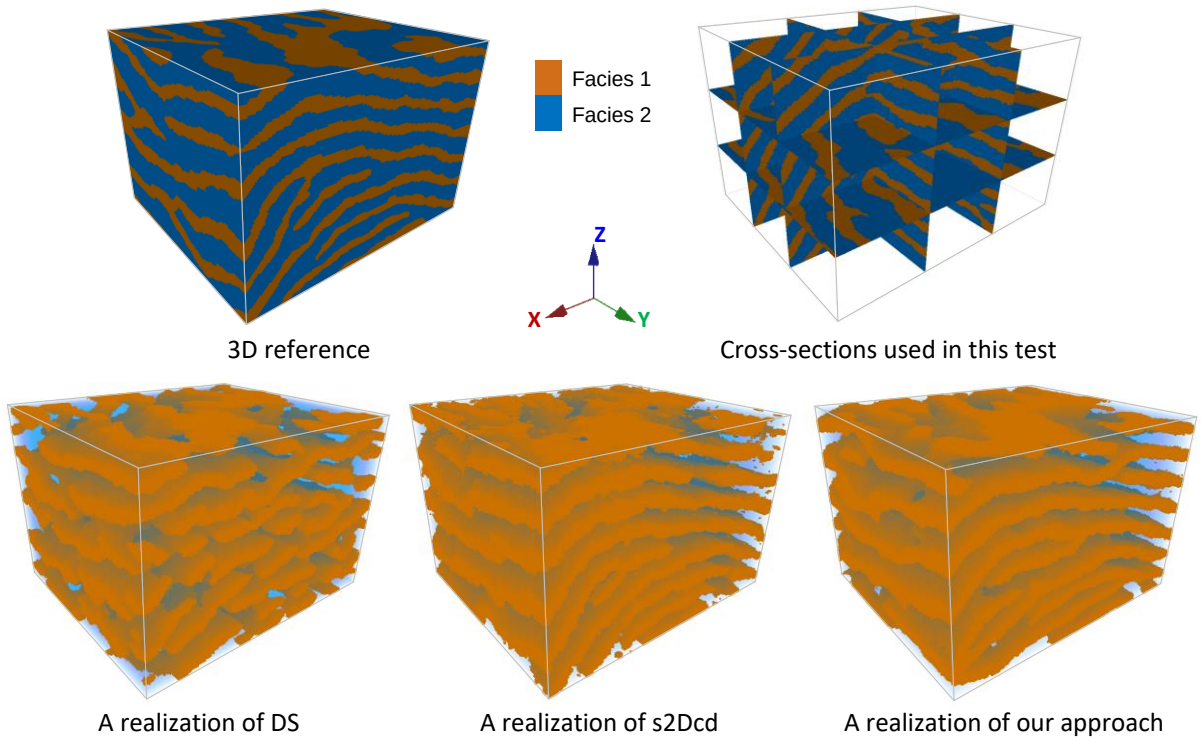

Figure 98. Realizations of three different MPS reconstruction methods. ~~In our method, the parameters.~~

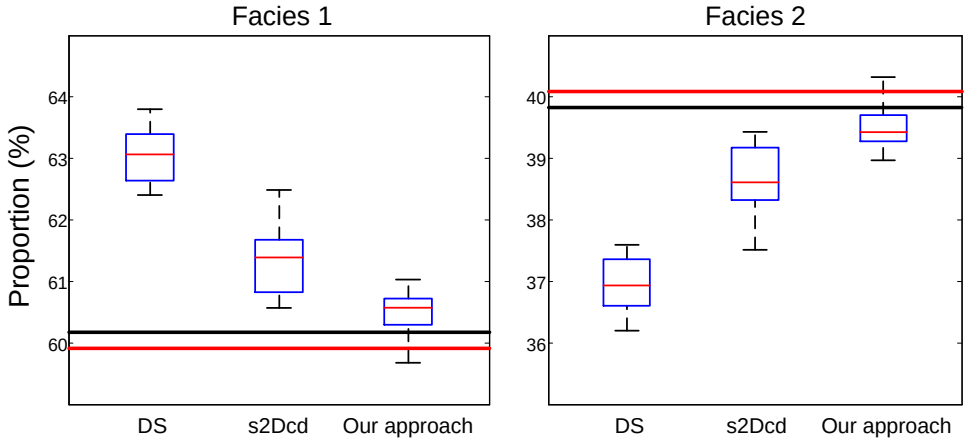

Figure 109. Proportions of the facies for 20 reconstructions by using three MPS methods. The black and red horizontal lines represent~~s~~ the proportions of facies in the 3-D reference and the cross-sections used as training images respectively.

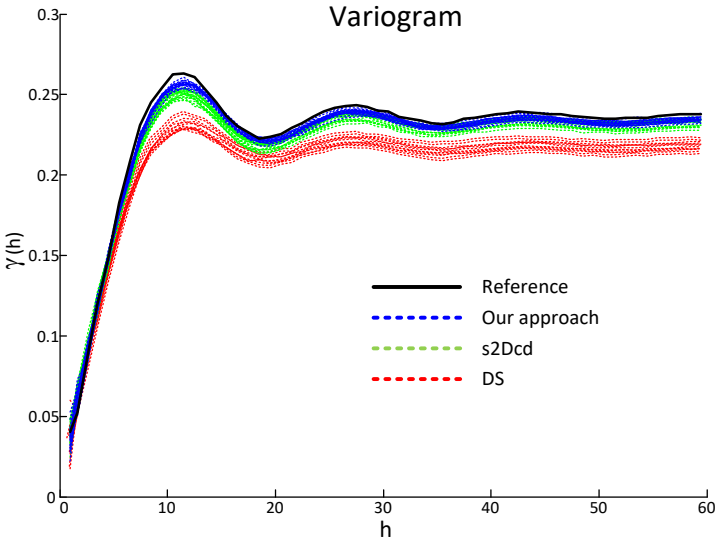

Figure 11~~10~~. Comparison of the variograms between DS, s2Dcd and our approach.

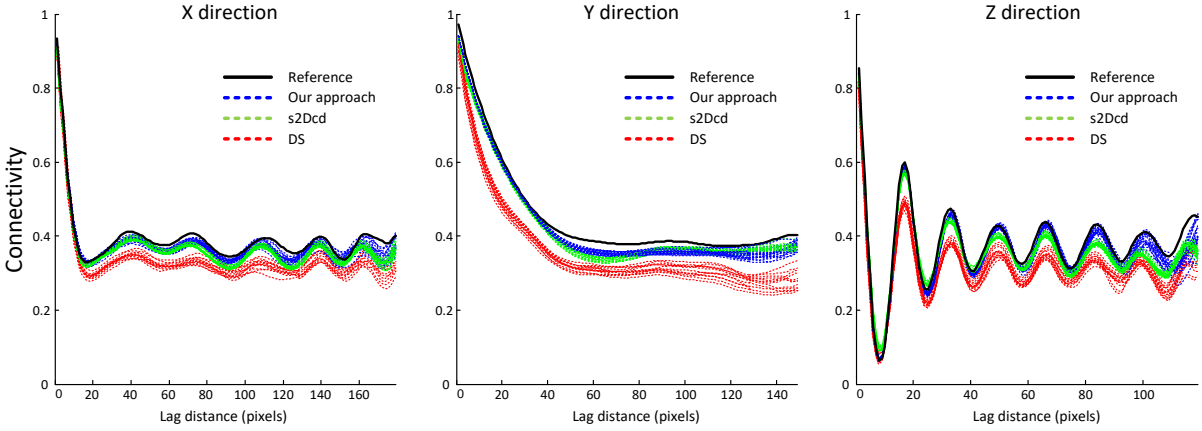

Figure 12~~11~~. Comparison of the connectivity functions in three directions with three MPS methods.

~~*Tan et al.* (2014) proposed a distance-based approach to evaluate the quality of MP simulation outcomes where the Jensen-Shannon (JS) divergence is used to depict the dissimilarity of MP histograms as a quantitative metric. The information in the dissimilarity of MP histograms can be visualized using multidimensional scaling (MDS) (*Caers*, 2011). MDS approximates these distances by a lower-dimensional Euclidean distance in Cartesian space, which facilitates the visualization of the dissimilarity of MP histograms.~~ To further compare the models obtained using the three different MPS approaches, MDS plots are constructed by calculating the distance of MP histograms between all the realizations of three approaches and a 3-D reference. The resulting MDS map is shown in Figure 13~~12~~ and it can be observed that the realizations of our method are closer to the reference in the MDS map than the results obtained by the other two approaches. In addition,

kernel smoothing is used to estimate the density distribution of the realizations of three different MPS approaches around the reference. The probabilities of the realizations are calculated from kernel density estimation by using the equation (4) described in section 2.3. According to the reference model, the three different approaches have quite similar probabilities with 29, 33, and 38% for DS, s2Dcd, and our approach, respectively. However, our approach still gains the highest probability.

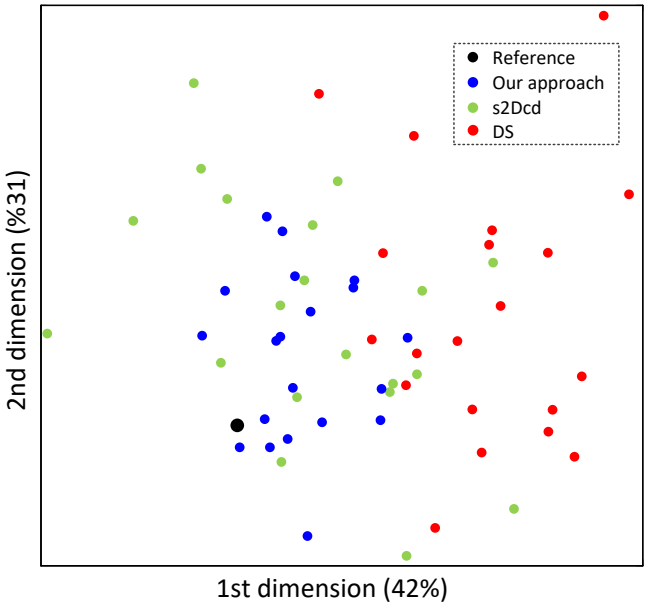

Figure 1312. MDS representation for 20 realizations of each MPS method.

In practice, there is no fully informed 3-D reference and we only have several informed cross-sections. Thus, the statistical features of the reconstructions (e.g. variograms, connectivity functions and MDS plots) are close to the reference but no one can surpass it in the above test. However, these comparisons are still able to validate the reproduction of spatial patterns for the different MPS approaches.

4.3. Computational Performance

~~In this section we focus on the analysis of computational performance. For the test illustrated in s~~Section 4~~3~~.1.1 and 4~~3~~.1.2 have already analyzed the influence of ~~, the average time per realization for different number of cross-sections, shown in Figure 13a, decreases rapidly with increasing~~ the number of cross-sections N_{cs} and ~~from one to six in each direction. Although this factor seriously affects the computational efficiency, we should strike a balance between the computational efficiency and variability of spatial patterns which is described in detail in section 3.1.2. For~~ the maximum of matched patterns from each training image $N_{\max}$. ~~depicted in section 3.1.2, the computational cost increases sharply in the first half~~

~~part by changing N_{max}, and then approximately tends to be stable (Figure 13b). Thus, a good choice for this factor is close to the turning point before the curve tends to be stable.~~ Section 4.1.4 tested the interaction between t, f, N_{cs} and N_{max}. The results indicated that the effect of t and f on the computational efficiency in our method is the same as in DS. The computational performance of other parameters has been assessed clearly by *Meerschman et al*. (2013). The weights of the probability aggregation formulas do not affect CPU time.

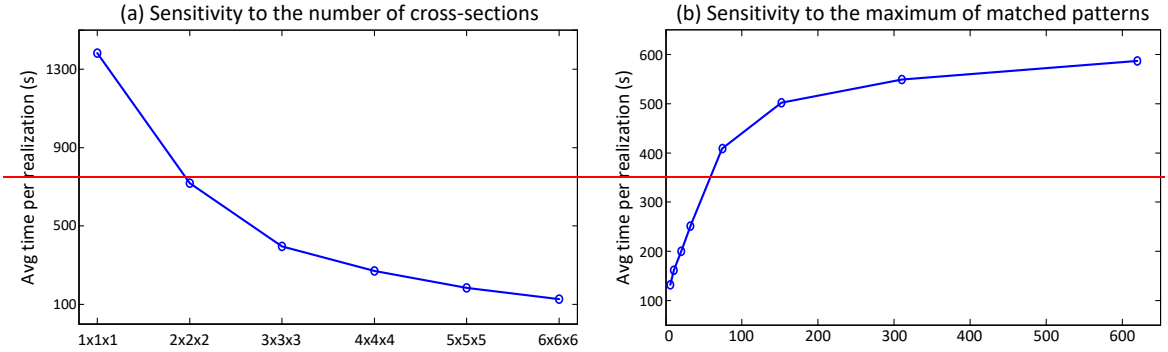

Figure 13. ~~Effect of (a) the number of cross-sections in each direction and (b) the maximum of matched patterns from each training image. The times are averaged on 20 realizations.~~

A comparison of computational performance between DS, s2Dcd and our approach is presented in Figure 14. Because our method is sensitive to the number of input cross-sections, we offer two and four sections in each direction respectively, and the computational efficiencies are shown in Figures 14a and 14b with increasing the total number of grid cells. Other parameters are the same as the test in section 3.2. Note that a different time axis is used for DS-based reconstruction because it uses much more CPU time than the other two methods, even though four processors are used for DS-based reconstruction. As shown in Figures 14a, ~~s2Dcd and~~ our approach presents ~~similar computational~~better computational performance ~~but much better~~ than DS-based 3-D reconstruction since the MP statistics are captured from a smaller domain composed of several 2-D sections in s2Dcd and our approach. Because four processors are used in DS and s2Dcd, thus our approach presents the speedups of about 4 compared to s2Dcd and about 120 compared to DS in this test (Figures 14a). When increasing the number of cross-sections, the search space is divided into more subdomains in our approach so as to achieve a much better performance than s2Dcd and DS (see Figure 14b).

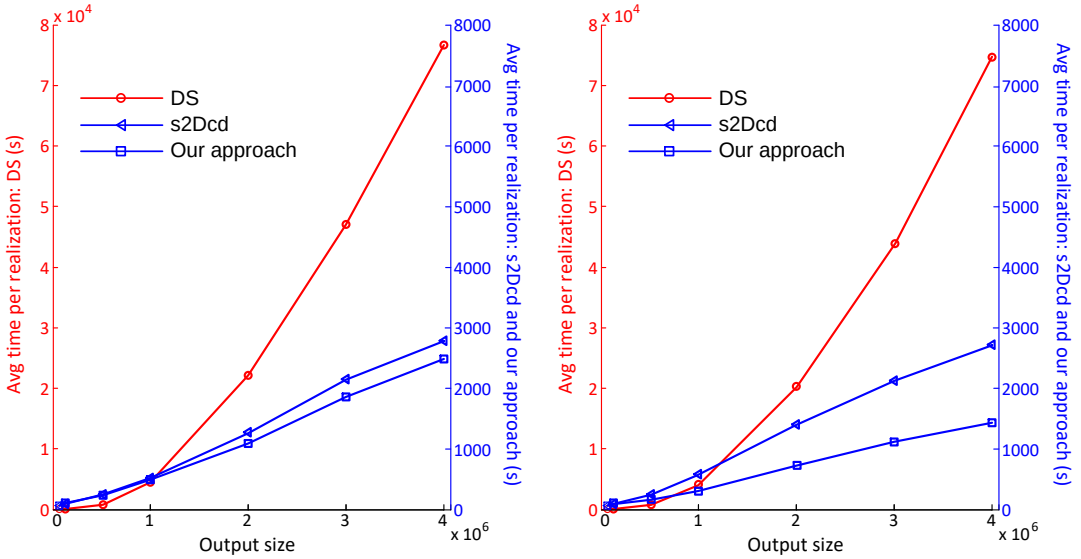

Figure 14. Comparison of computational performance between DS, s2Dcd and our approach with increasing the size of output grid: (left) two cross-sections and (right) four cross-sections in each direction. Note that different time axises are used in the two subplots, and four processors are used for DS-based reconstruction and s2Dcd but only one for our method.

5. Synthetic Example: 3-D Reconstruction of Hydrofacies ~~Application Example~~

To further demonstrate the applicability of our algorithm, an example from a real geological application is presented in this section. The Descalvado aquifer analog dataset (Figure 15) depicts the complex hydrofacies of a small area (28m × 7m × 5.8m) in Brazil (*Bayer et al.*, 2015). In the original dataset, there are five cross-sections derived from outcrops, which are marked by black lines in Figure 15a. They are referenced in a 3-D domain consisting of 280 × 70 × 58 voxels. These sections allow creating only two parts ~~so~~ of subdomains, which is insufficient for an application of our method. Therefore, we borrow the strategy of *Gueting et al*. (2017) to insert three additional sections in yz direction using sequential 2-D MP simulation approach (s2Dcd) firstly which are marked by blue lines in Figure 15a. Then, all the tests are implemented on the basis of eight cross-sections (three in xz direction and five in yz direction) which are shown in Figure 15b.

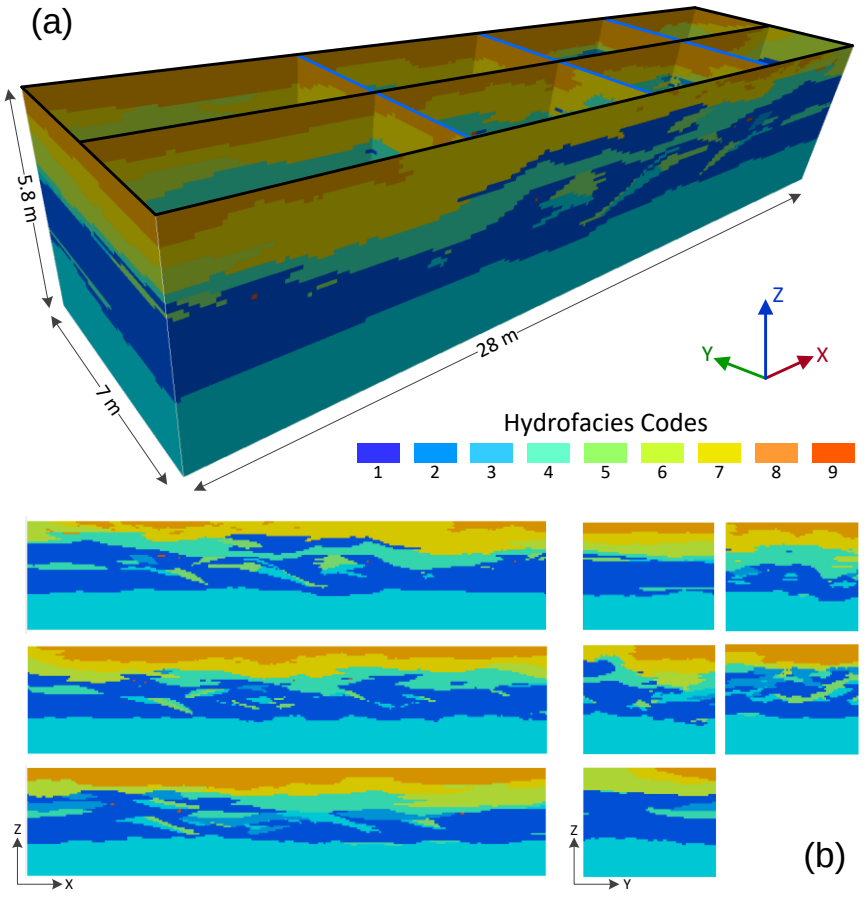

Figure 15. Descalvado aquifer analog dataset (*Bayer et al.*, 2015). (a) 3-D presentation of the informed cross-sections: three sections in xz direction, and five sections in yz direction; (b) 2-D presentation of these informed sections.

Figure 16 shows realizations obtained by using three different MPS approaches on the basis of the above-mentioned dataset. The white lines indicate the locations of informed sections in each realization. Note that an auxiliary variable along the *z* coordinate is used in s2Dcd and our approach. It is a continuous variable to control the changing trend of the hydrofacies along the *z* coordinate and the detailed description is given by *Comunian et al.* (2012). To further reveal the performance of the different approaches, we use MDS maps to visualize the dissimilarity of MP histograms (Figure 17), similarly as in section 4.2. However here we use it to reveal the dissimilarity between all the reconstructed sections exacted from the realizations and the eight informed sections along the two directions, rather than different 3-D realizations. Thus, for each realization, 70 sections (67 reconstructed sections and 3 informed sections) from *xz* direction and 280 sections (275 reconstructed sections and 5 informed sections) from *yz* direction are used to draw the MDS maps along the two directions respectively. MDS is very appropriate to present the dissimilarity for this kind of applications because we only have partial cross-sections instead of an entire 3-D training image. Therefore, it is necessary to assess the dissimilarity between the

reconstructed sections and informed sections. As shown in Figure 15, the sections from *xz* and *yz* directions are very different, such as the correlation lengths and the complexity of structures. Thus, we draw different MDS maps respectively for the *xz* and *yz* directions (Figures ~~16a~~ 17a and ~~16b~~17b). Individual sections from the realizations are compared in Figures ~~16c~~ 17c and ~~16d~~17d. Overall, it can be observed both visually and in the MDS maps that the sections obtained from our approach are closest to the informed sections.

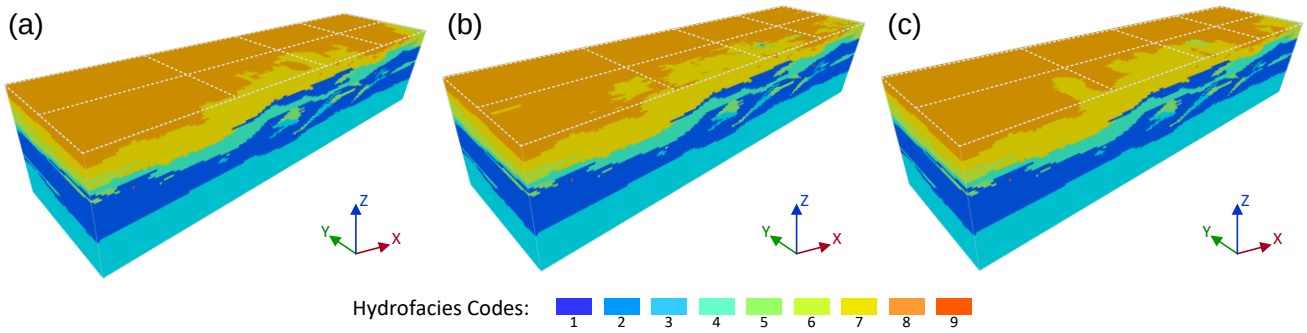

Figure 16. Three realizations using three different MPS approaches: (a) DS, (b) s2Dcd with the coordinate z as auxiliary variable; and (c) our approach with the coordinate z as auxiliary variable.

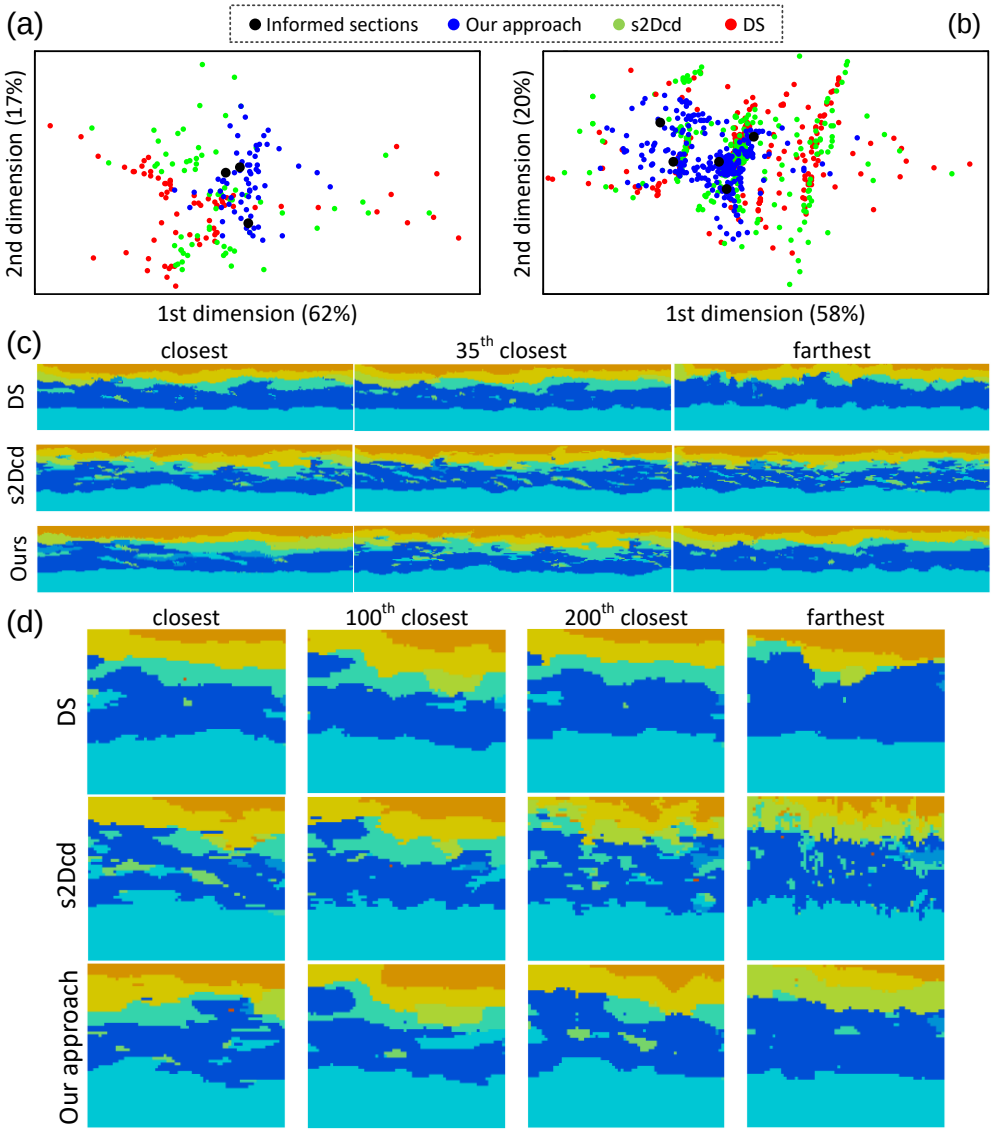

Figure 17. MDS maps of sections extracted from realizations using three different MPS approach. (a) MDS map of 70 sections for each realization along *xz* direction; (b) MDS map of 280 sections for each realization along *yz* direction; (c) selected sections for each method according to the JS divergence in *xz* direction; (d) selected sections in *yz* direction.

Our method is able to reduce the non-stationarity effect of real geological data to a certain extent due to the local search strategy. As shown in the above analysis, the patterns in the informed cross-sections are very complicated where the distribution of hydrofacies is anisotropic and non-stationary, especially for the facies with a lower proportion. As illustrated in Figure 18a, a local domain is surrounded by four segments from the informed cross-sections. It should be noted that there is no facies 2 in all the four segments. We extract the local parts from three realizations by using different MPS approaches.

Then we check all the segments of the three local models, and we find that facies 2 is reproduced in this local area in the realizations of DS and s2Dcd. Three segments are randomly selected from the three local models, and they are shown in Figure 18b where the boundaries of facies 2 are marked by red lines. Figure 18c shows the histograms of the four informed segments and the local models of 10 realizations for each MPS method. It can be observed that, although there is no facies 2 in the closest four segments, it is reproduced in this local area by DS and s2Dcd. Conversely, our approach can maintain the distribution of facies well since all the MP statistics are captured from the surrounded sub-sections. If the surrounding sub-sections of a local area do not contain an attribute but it exists in other locations, the patterns with this attribute will not be moved to this local area in our approach. This indicates that our approach allows involving the non-stationary geological analogs in the 3-D real applications, and spatial patterns are restricted into a local domain so that they are not carried to faraway locations.

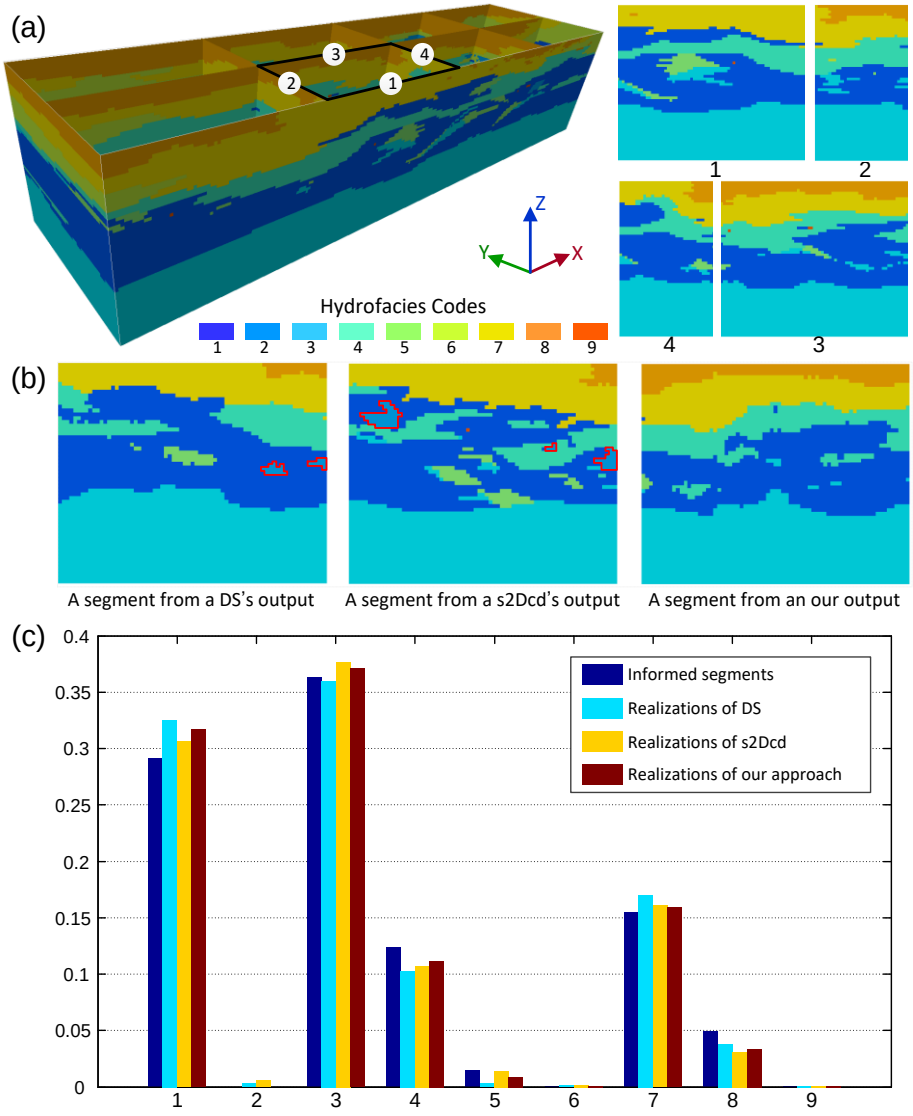

Figure 18. Comparison of reproduction of non-stationary patterns. (a) a local domain and the four corresponding segments; (b) three selected segments from the realizations obtained using different approaches in the local area; (c) histograms of the four informed segments and the ~~three~~ local models of 10 realizations for each MPS method.

In the real-world applications, the geological sections or other analogs are not always straight or orthogonal. Therefore we need to project them in orthogonal directions. Figure 19 illustrates the process of projecting the tortuous sections to the parallel planes along a given direction. The same strategy can be used to address the issues in other directions. After that the original sections will be used as hard data and the projected sections will be only as training images. Thus other scattered samples (e.g. boreholes, outcrops) also can be involved as hard data.

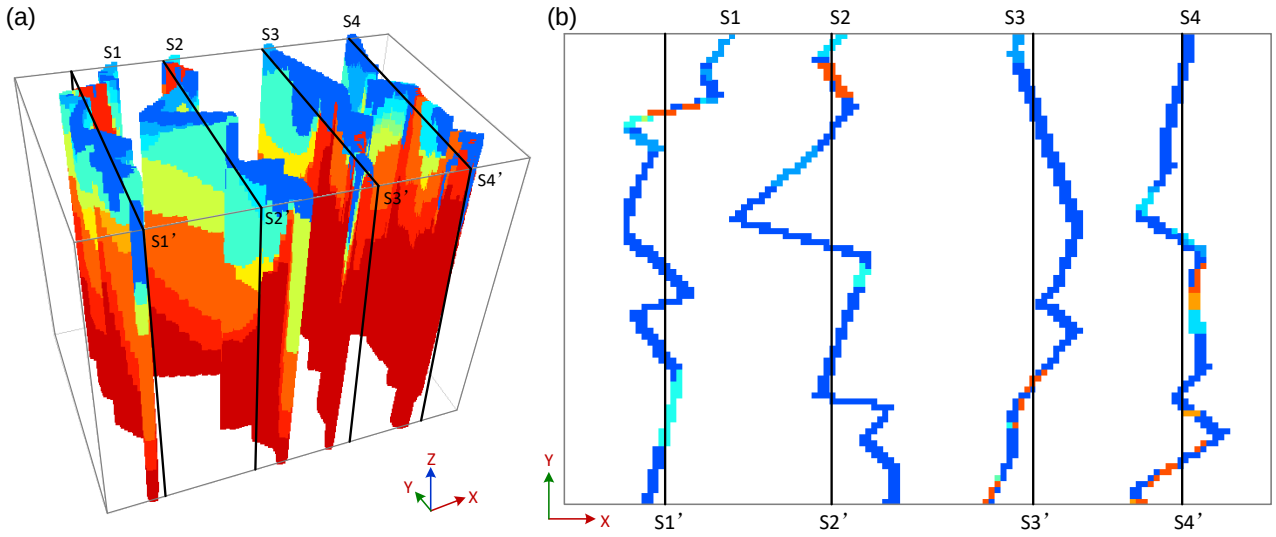

Figure 19. Process of projecting real-world sections to parallel planes along a given direction: the process in (a) 3-D space and (b) xy plane.

6. Discussion and Conclusion

In this paper, we presented a novel method for reconstructing 3-D complex heterogeneous structures by using partial lower dimensional data. Indeed, this is a very general issue since inferring high-dimensional patterns from low-dimensional data (e.g. boreholes, outcrops and other analogs) is a very common workflow for geologists. In practice, reliable 3-D models of complex geological structures are still difficult to construct due to the heterogeneity of geological phenomena and processes, even though there are many real geological analogs or sections that can be used. Our method makes it possible to reconstruct 3-D structures with MPS when no 3-D training image is available. The synthetic experiments and practical applications presented in this paper demonstrate the capacity to reconstruct such heterogeneous structures.

As compared to the previous MPS implementations that use partial data, the proposed method requires several local training sub-sections surrounding a simulated node, rather than a full section (*Comunian et al.*, 2012) or points in a 3-D domain (*Mariethoz and Renard*, 2010). The local search strategy proposed in this paper allows to compute more reliable MP statistics because it avoids that spatial patterns from faraway locations are considered in the simulation of the current node. In this strategy, the original cross-sections are divided into many sub-sections according to their spatial relationships. Therefore, the non-stationarity of real geological analogs is reduced to a certain extent because the training patterns cannot be borrowed from further than a local subdomain. Of course, besides cross-sections, other scattered samples also can be included as hard data.

Moreover, our approach increases the computational efficiency compared with existing MPS methods. The local search strategy allows acquiring MP statistics from the local sub-sections so that the searches are significantly reduced. Its good

computational performance makes it potentially applicable to real 3-D modeling problems such as porous media, hydrofacies, reservoir, and other complex sedimentary structures. In addition, a new parameter, the maximum of matched patterns from each training image is adopted to avoid the unnecessary searches. The experimental results demonstrated that a reasonable choice for this parameter can not only ensure to capture a stable cpdf, but also gain a further performance speed-up.

The method presented here retains many advantages of DS (*Mariethoz et al*., 2010), such as unnecessary storing for MP statistics, pattern distances, flexible neighborhood. Nevertheless, we propose an adaptive and flexible implementation of the search template on multiple grids where the radius of the neighborhood, the distance threshold and the size of data events decrease linearly with the rising of levels of multiple grids. As a result, a big data event is divided into several small parts placed on the different grids, which results in a smaller neighborhood on each grid. An acceptable distance threshold is assigned to the first grid to make it easier to obtain a stable cpdf and to capture the large-scale features from the original sparse samples. For the last grid, the radius of neighborhood is reduced to one and the highest criterion is carried out for the threshold (i.e. $t = 0$) which avoids the small-scale features or lower proportion facies are filtered out. Hence, the simulation of each multi-grid is simulated with different parameters, allowing for flexibility in simulating different structures at different scales.

Another important advantage of our approach is the probability aggregation strategy where the combinations of two different formulas are used to combine the cpdfs from different sub-sections. First, an additive aggregation method, linear pooling formula is used to combine two disjunctive probability distributions from each pair of parallel sub-sections to obtain a more stable pdf. The weights of this step are related to the distances between the current location and the two parallel sub-sections. Such parameterization is able to ensure the pattern trend changing from one sub-section to another one. And then, we aggregate the orthogonal pdfs and prior probability distribution by using a multiplicative method, log-linear pooling formula. This step can enhance the capability for reconstructing connectivity of spatial patterns in comparison with the method using a series of 2-D MPS simulations to fill a 3-D domain along given orthogonal directions (*Comunian et al.*, 2012).

The limitations of our method come from that it is not always possible to obtain abundant sections in each direction, and extremely small local blocks cannot offer enough spatial patterns, thus a minimal sub-section size has to be considered. In addition, our method is not able to perform the simulation of continuous variables. The proposed method can be further improved to overcome these limitations. Another possible direction is to parallelize the proposed MPS implementation and further enhance its computational performance.

*Competing interests***.** The authors declare that they have no conflict of interest.

Acknowledgments

We are grateful to three anonymous reviewers for their insightful comments and suggestions which led to the improvements in the manuscript. This work was supported in part by the National Natural Science Foundation of China (U1711267, 41172300) and the Ministry of Education Key Laboratory of Geological Survey and Evaluation (CUG2019ZR03). The authors wish to thank Philippe Renard and Julien Straubhaar for providing the MPS algorithm DeeSse; Moctar Dembele, Min Zeng and Luiz Gustavo Rasera for the fruitful discussions. An executable program of the proposed algorithm is available on the website of the first author (http://www.escience.cn/people/chenqiyu/index.html), and the source code developed by using C++ is available on request from the first author (qiyu.chen@cug.edu.cn).

References

Allard, D., Comunian, A., and Renard, P.: Probability aggregation methods in geoscience, *Mathematical Geosciences*, 44, 545-581, 2012.

Arpat, G. B., and Caers, J.: Conditional simulation with patterns. *Mathematical Geology*, 39(2), 177-203, 2007.

Bayer, P., Comunian, A., Höyng, D., and Mariethoz, G.: High resolution multi-facies realizations of sedimentary reservoir and aquifer analogs, *Scientific Data*, 2, 150033, 2015.

Bayer, P., Huggenberger, P., Renard, P., and Comunian, A.: Three-dimensional high resolution fluvio-glacial aquifer analog: Part 1: Field study, *Journal of Hydrology*, 405, 1-9, 2011.

Bordley, R. F.: A multiplicative formula for aggregating probability assessments, *Management Science*, 28, 1137-1148, 1982.

Caers, J.: Geostatistical reservoir modelling using statistical pattern recognition, *Journal of Petroleum Science and Engineering*, 29, 177-188, 2001.

Caers, J.: Modeling uncertainty in the earth sciences. Wiley, Hoboken, 2011.

Chen, Q., Liu, G., Li, X., Zhang, Z., and Li, Y.: A corner-point-grid-based voxelization method for the complex geological structure model with folds, *Journal of Visualization*, 20, 875-888, 2017.

Chugunova, T. L., and Hu, L. Y.: Multiple-point simulations constrained by continuous auxiliary data, *Mathematical Geosciences*, 40, 133-146, 2008.

Comunian, A., Renard, P., and Straubhaar, J.: 3-D multiple-point statistics simulation using 2-D training images, *Computers & Geosciences*, 40, 49-65, 2012.

Comunian, A., Renard, P., Straubhaar, J., and Bayer, P.: Three-dimensional high resolution fluvio-glacial aquifer analog – Part 2: Geostatistical modeling, *Journal of Hydrology*, 405, 10-23, 2011.

Comunian, A., Jha, S. K., Giambastiani, B. M. S., Mariethoz, G., and Kelly, B. F. J.: Training Images from Process-Imitating Methods, *Mathematical Geosciences*, 46, 241-260, 2014.

Caumon, G., Collon-Drouaillet, P., De Veslud, C. L. C., Viseur, S., and Sausse, J.: Surface-based 3-D modeling of geological structures, *Mathematical Geosciences*, 41(8), 927-945, 2009.

Dai, Z., Ritzi, R. W., and Dominic, D. F.: Improving permeability semivariograms with transition probability models of hierarchical sedimentary architecture derived from outcrop analog studies, *Water Resources Research*, 41, 2005.

Deutsch, C. V., and Tran, T. T.: FLUVSIM: a program for object-based stochastic modeling of fluvial depositional systems, *Computers & Geosciences*, 28(4), 525-535, 2002.

de Marsily, G., Delay, F., Gonçalvès, J., Renard, P., Teles, V., and Violette, S.: Dealing with spatial heterogeneity, *Hydrogeology Journal*, 13, 161-183, 2005.

de Vries, L. M., Carrera, J., Falivene, O., Gratacós, O., and Slooten, L. J.: Application of multiple point geostatistics to non-stationary images, *Mathematical Geosciences*, 41, 29-42, 2009.

Dell Arciprete, D., Bersezio, R., Felletti, F., Giudici, M., Comunian, A., and Renard, P.: Comparison of three geostatistical methods for hydrofacies simulation: a test on alluvial sediments, *Hydrogeology Journal*, 20, 299-311, 2012.

Feyen, L., and Caers, J.: Multiple-point geostatistics: a powerful tool to improve groundwater flow and transport predictions in multi-modal formations. In: Renard, P., Demougeot-Renard, H., Froidevaux, R. (Eds.), *GeoENV V: Geostatistics for Environmental Applications*. Springer, Berlin Heidelberg, pp. 197–208, 2004.

Foged, N., Marker, P. A., Christansen, A. V., Bauer-Gottwein, P., Jørgensen, F., Høyer, A.-S., and Auken, E.: Large-scale 3-D modeling by integration of resistivity models and borehole data through inversion, *Hydrology and Earth System Sciences*, 18, 4349-4362, 2014.

Gaud, M. N., Smith, G. A., and McKenna, S. A.: Relating small-scale permeability heterogeneity to lithofacies distribution, In: Bridge, J., and D. W. Hyndman (Eds.), *Aquifer Characterization*, vol. 80. SEPM, Special Publication, pp. 55-66, 2004.

Genest, C., and Zidek, J. V.: Combining probability distributions: A critique and an annotated bibliography, *Statistical Science*, 114-135, 1986.

Guardiano, F. B., and Srivastava, R. M.: Multivariate geostatistics: beyond bivariate moments. In *Geostatistics Troia'92*. Springer Netherlands, pp. 133-144, 1993.

Gueting, N., Caers, J., Comunian, A., Vanderborght, J., and Englert, A.: Reconstruction of three-dimensional aquifer heterogeneity from two-dimensional geophysical data. *Mathematical Geosciences*, 50(1), 53-75, 2017.

Hajizadeh, A., Safekordi, A., and Farhadpour, F. A.: A multiple-point statistics algorithm for 3-D pore space reconstruction from 2-D images, *Advances in Water Resources*, 34, 1256-1267, 2011.

He, X. L., Sonnenborg, T. O., Jørgensen, F., and Jensen, K. H.: The effect of training image and secondary data integration with multiple-point geostatistics in groundwater modelling, *Hydrology and Earth System Sciences*, 18, 2943-2954, 2014.

Heinz, J., Kleineidam, S., Teutsch, G., and Aigner, T.: Heterogeneity patterns of Quaternary glaciofluvial gravel bodies (SW-Germany): application to hydrogeology. *Sedimentary geology*, 158(1), 1-23, 2003.

Hermans, T., Nguyen, F., and Caers, J.: Uncertainty in training image-based inversion of hydraulic head data constrained to ERT data: Workflow and case study, *Water Resources Research*, 51, 5332-5352, 2015.

Hoffman, B. T., and Caers, J.: History matching by jointly perturbing local facies proportions and their spatial distribution: Application to a North Sea reservoir, *Journal of Petroleum Science and Engineering*, 57(3), 257-272, 2007.

~~Honarkhah, M., and Caers, J.: Stochastic simulation of patterns using distance based pattern modeling, *Mathematical Geosciences*, 42, 487-517, 2010.~~

Høyer, A.-S., Vignoli, G., Hansen, T. M., Vu, L. T., Keefer, D. A., and Jørgensen, F.: Multiple-point statistical simulation for hydrogeological models: 3-D training image development and conditioning strategies, *Hydrology and Earth System Sciences*, 21, 6069-6089, 2017.

Hu, L. Y., and Chugunova, T.: Multiple-point geostatistics for modeling subsurface heterogeneity: A comprehensive review, *Water Resources Research*, 44, 2008.

Hu, R., Brauchler, R., Herold, M., and Bayer, P.: Hydraulic tomography analog outcrop study: Combining travel time and steady shape inversion, *Journal of Hydrology*, 409, 350-362, 2011.

Huysmans, M., Orban, P., Cochet, E., Possemiers, M., Ronchi, B., Lauriks, K., Batelaan, O., and Dassargues, A.: Using multiple-point geostatistics for tracer test modeling in a clay-drape environment with spatially variable conductivity and sorption coefficient, *Mathematical Geosciences*, 46, 519-537, 2014.

Jackson, M. D., Percival, J. R. , Mostaghiml, P., Tollit, B. S., Pavlidis, D., Pain, C. C., Gomes, J. L. M. A., El-Sheikh, A. H., Salinas, P., Muggeridge, A. H., and Blunt, M. J.: Reservoir modeling for flow simulation by use of surfaces, adaptive unstructured meshes, and an overlapping-control-volume finite-element method, *SPE Reservoir Evaluation & Engineering*, 18, 115-132, 2015.

Jha, S. K., Comunian, A., Mariethoz, G., and Kelly, B. F. J.: Parameterization of training images for aquifer 3-D facies modeling integrating geological interpretations and statistical inference, *Water Resources Research*, 50, 7731-7749, 2014.

~~Journel, A. G.: Geostatistics: roadblocks and challenges, In *Geostatistics Troia'92*. Springer Netherlands, pp. 213-224, 1993.~~

Journel, A. G.: Combining knowledge from diverse sources: An alternative to traditional data independence hypotheses, *Mathematical Geology*, 34, 573-596, 2002.

Kessler, T. C., Comunian, A., Oriani, F., Renard, P., Nilsson, B., Klint, K. E., and Bjerg, P. L.: Modeling Fine-Scale Geological Heterogeneity-Examples of Sand Lenses in Tills, *Ground Water*, 51, 692-705, 2013.

Klise, K. A., Weissmann, G. S., McKenna, S. A., Nichols, E. M., Frechette, J. D., Wawrzyniec, T. F., and Tidwell, V. C.: Exploring solute transport and streamline connectivity using lidar-based outcrop images and geostatistical representations of heterogeneity, *Water Resources Research*, 45(5), 2009.

Knudby, C., and Carrera, J.: On the relationship between indicators of geostatistical, flow and transport connectivity. *Advances in Water Resources*, 28(4), 405-421, 2005.

Krishnan, S.: The Tau Model for Data Redundancy and Information Combination in Earth Sciences: Theory and Application, *Mathematical Geosciences*, 40, 705-727, 2008.

~~Lee, S. Y., Carle, S. F., and Fogg, G. E.: Geologic heterogeneity and a comparison of two geostatistical models: Sequential Gaussian and transition probability based geostatistical simulation, *Advances in water resources*, 30(9), 1914-1932, 2007.~~

~~Li, X., Mariethoz, G., Lu, D., and Linde, N.: Patch based iterative conditional geostatistical simulation using graph cuts, *Water Resources Research*, 52, 6297-6320, 2016.~~

Maharaja, A.: TiGenerator: Object-based training image generator, *Computers & Geosciences*, 34, 1753-1761, 2008.

Mahmud, K., Mariethoz, G., Baker, A., and Sharma, A.: Integrating multiple scales of hydraulic conductivity measurements in training image-based stochastic models, *Water Resources Research*, 51, 465-480, 2015.

~~Mahmud, K., Mariethoz, G., Caers, J., Tahmasebi, P., and Baker, A.: Simulation of Earth textures by conditional image quilting, *Water Resources Research*, 50, 3088-3107, 2014.~~

Mariethoz, G., and Kelly, B. F. J.: Modeling complex geological structures with elementary training images and transform-invariant distances, *Water Resources Research*, 47(7), 2011.

Mariethoz, G., and Renard, P.: Reconstruction of incomplete data sets or images using direct sampling, *Mathematical Geosciences*, 42, 245-268, 2010.

Mariethoz, G., Straubhaar, J., Renard, P., Chugunova, T., and Biver, P.: Constraining distance-based multipoint simulations to proportions and trends, *Environmental Modelling & Software*, 72, 184-197, 2015.

Mariethoz, G., Renard, P., and Straubhaar, J.: The Direct Sampling method to perform multiple-point geostatistical simulations, *Water Resources Research*, 46(11), 2010.

Mariethoz, G., Renard, P., and Froidevaux, R.: Integrating collocated auxiliary parameters in geostatistical simulations using joint probability distributions and probability aggregation, *Water Resources Research*, 45(8), 2009.

Meerschman, E., Pirot, G., Mariethoz, G., Straubhaar, J., Van Meirvenne, M., and Renard, P.: A practical guide to performing multiple-point statistical simulations with the Direct Sampling algorithm. *Computers & Geosciences*, 52, 307-324, 2013.

Nichols, E. M., Weissmann, G. S., Wawrzyniec, T. F., Frechette, J. D., and Klise, K. A.: Processing of outcrop-based lidar imagery to characterize heterogeneity for groundwater models, *SEPM concepts in sedimentology and paleontology*, 10, 239-47, 2011.

~~Okabe, H., and Blunt, M.J.: Pore space reconstruction using multiple point statistics, *Journal of Petroleum Science and Engineering*, 46, 121-137, 2005.~~

Okabe, H., and Blunt, M. J.: Pore space reconstruction of vuggy carbonates using microtomography and multiple-point statistics, *Water Resources Research*, 43(12), 2007.

Oriani, F., Straubhaar, J., Renard, P., and Mariethoz, G.: Simulation of rainfall time series from different climatic regions using the direct sampling technique, *Hydrology and Earth System Sciences*, 18, 3015-3031, 2014.

~~Phelps, G., and Boucher, A.: Mapping locally complex geologic units in three dimensions: the multi point geostatistical approach, *Three-Dimensional Geological Mapping*, 36-39, 2009.~~

Pickel, A., Frechette, J. D., Comunian, A., and Weissmann, G. S.: Building a training image with Digital Outcrop Models, *Journal of Hydrology*, 531, 53-61, 2015.

Pirot, G., Straubhaar, J., and Renard, P.: A pseudo genetic model of coarse braided-river deposits, *Water Resources Research*, 51, 9595-9611, 2015.

Pyrcz, M. J., Boisvert, J. B., and Deutsch, C. V.: ALLUVSIM: A program for event-based stochastic modeling of fluvial depositional systems, *Computers & Geosciences*, 35(8), 1671-1685, 2009.

Pyrcz, M. J., and Deutsch, C. V.: Geostatistical reservoir modeling. Oxford university press, 2014.

Raiber, M., White, P. A., Daughney, C. J., Tschritter, C., Davidson, P., and Bainbridge, S. E.: Three-dimensional geological modelling and multivariate statistical analysis of water chemistry data to analyse and visualise aquifer structure and groundwater composition in the Wairau Plain, Marlborough District, New Zealand, *Journal of Hydrology*, 436-437, 13-34, 2012.

Renard, P., and Allard, D.: Connectivity metrics for subsurface flow and transport. *Advances in Water Resources*, 51, 168-196, 2013.

Ritzi, R. W.: Behavior of indicator variograms and transition probabilities in relation to the variance in lengths of hydrofacies, *Water resources research*, 36(11), 3375-3381, 2000.

Stone, M.: The opinion pool. *The Annals of Mathematical Statistics*, 32(4), 1339-1342, 1961.

Straubhaar, J., Renard, P., Mariethoz, G., Froidevaux, R., and Besson, O.: An improved parallel multiple-point algorithm using a list approach, *Mathematical Geosciences*, 43(3), 305-328, 2011.

Strebelle, S.: Conditional simulation of complex geological structures using multiple-point statistics, *Mathematical Geology*, 34, 1-21, 2002.

Tahmasebi, P., Hezarkhani, A., and Sahimi, M.: Multiple-point geostatistical modeling based on the cross-correlation functions, *Computational Geosciences*, 16, 779-797, 2012.

~~Tahmasebi, P., Sahimi, M., and Caers, J.: MS-CCSIM: Accelerating pattern-based geostatistical simulation of categorical variables using a multi-scale search in Fourier space, *Computers & Geosciences*, 67, 75-88, 2014.~~

Tran, T. T.: Improving variogram reproduction on dense simulation grids. *Computers & Geosciences*, 20(7-8), 1161-1168, 1994.

Vassena, C., Cattaneo, L., and Giudici, M.: Assessment of the role of facies heterogeneity at the fine scale by numerical transport experiments and connectivity indicators, *Hydrogeology Journal*, 18(3), 651-668, 2010.

Wambeke, T., and Benndorf, J.: An integrated approach to simulate and validate orebody realizations with complex trends: A case study in heavy mineral sands, *Mathematical Geosciences*, 48, 767-789, 2016.

Weissmann, G. S., Carle, S. F., and Fogg, G. E.: Three-dimensional hydrofacies modeling based on soil surveys and transition probability geostatistics, *Water Resources Research*, 35(6), 1761-1770, 1999.

Weissmann, G. S., Pickel, A., McNamara, K. C., Frechette, J. D., Kalinovich, I., Allen-King, R. M., and Jankovic, I.: Characterization and quantification of aquifer heterogeneity using outcrop analogs at the Canadian Forces Base Borden, Ontario, Canada, *Geological Society of America Bulletin*, 127(7-8), 1021-1035, 2015.

Wu, J., Boucher, A., and Zhang, T.: A SGeMS code for pattern simulation of continuous and categorical variables: FILTERSIM, *Computers & Geosciences*, 34, 1863-1876, 2008.

Wu, K., Van Dijke, M. I. J., Couples, G. D., Jiang, Z., Ma, J., Sorbie, K. S., Crawford, J., Young, I., and Zhang, X.: 3-D stochastic modelling of heterogeneous porous media – Applications to reservoir rocks, *Transport in Porous Media*, 65, 443-467, 2006.

Yang, L., Hou, W., Cui, C., and Cui, J.: GOSIM: A multi-scale iterative multiple-point statistics algorithm with global optimization, *Computers & Geosciences*, 89, 57-70, 2016.

Zappa, G., Bersezio, R., Felletti, F., and Giudici, M. Modeling heterogeneity of gravel-sand, braided stream, alluvial aquifers at the facies scale, *Journal of Hydrology*, 325, 134-153, 2006.

Zhang, T., Li, D., Lu, D., and Yang, J.: Research on the reconstruction method of porous media using multiple-point geostatistics, *Science China Physics, Mechanics and Astronomy*, 53, 122-134, 2010.

Zhang, T., Switzer, P., and Journel, A.: Filter-based classification of training image patterns for spatial simulation, *Mathematical Geology*, 38, 63-80, 2006.